Projections from thalamic nucleus reuniens to hippocampal CA1 area enable context value updating

Authors

Magdalena Ziółkowska, Narges Sotoudeh, Anna Cały, Monika Puchalska, Roberto Pagano[&], Małgorzata Alicja Śliwińska[#], Ahmad Salamian and Kasia Radwanska*****

Affiliation

Laboratory of Molecular Basis of Behavior, Nencki Institute of Experimental Biology of Polish Academy of Sciences, 3 Pasteur St., Warsaw 02-093, Poland.

[&] currently Laboratory of Molecular and Cellular Neurobiology, International Institute of Molecular and Cell Biology, Warsaw, Poland

[#] currently Electron Microscopy Platform & Bio Imaging Core at VIB-KU Leuven Center for Brain and Disease Research, and Department of Neurosciences at KU Leuven, Campus Gasthuisberg, building O&N5, Herestraat 49 box 602, 3000 Leuven, Belgium.

***Corresponding author:** Kasia Radwanska, Ph.D., Laboratory of Molecular Basis of Behavior, the Nencki Institute of Experimental Biology of Polish Academy of Sciences, 3 Pasteur St., Warsaw 02-093, Poland; e-mail: k.radwanska@nencki.edu.pl; tel: +48 501 736 942.

Abstract

The ability to extinguish contextual fear in a changing environment is crucial for animal survival. The 'classic' neuronal circuit of contextual fear extinction includes the medial prefrontal cortex (mPFC), amygdala, and hippocampus. However, recent data also support the role of the thalamic nucleus reuniens (RE) in this process. Here, we aimed to determine whether the projections from RE to the dorsal hippocampal CA1 area (RE→dCA1) play a role in updating context-dependent memories and to characterize the underlying synaptic processes. We used chemogenetic manipulations and conducted *ex vivo* field recordings in mice to analyze the impact of RE afferents on synaptic transmission in the dCA1. Next, we employed virally mediated labeling of RE afferents in Thy1-GFP mice to analyze the RE buttons and dendritic spines (as a proxy for glutamatergic synapses) in dCA1 during contextual fear memory extinction. This approach was complemented by 3D electron microscopy to analyze synaptic changes with nano-scale resolution. Finally, using projection-specific chemogenetic manipulation, we tested the role of the RE→CA1 projection in the classic contextual fear extinction paradigm, as well as in the extinction of aversive and appetitive contextual memories in a close-to-ecological environment of IntelliCages. Overall, our data demonstrate that RE regulates synaptic transmission in the stratum oriens (SO) and lacunosum-moleculare of the CA1 area (SLM). Extinction of contextual fear induces synaptic plasticity in these regions. However, only the changes in SLM are specific for the dendrites innervated by RE. Finally, we demonstrate that the RE→dCA1 pathway contributes to updating contextual memories independent of their valence.

Introduction

The distinction between dangerous and safe contexts, as well as the ability to update such information in a changing environment, is crucial for animal survival, as mistakes can have costly consequences. Impairments in context-dependent behaviors have been associated with pathological conditions such as post-traumatic stress disorder, schizophrenia, and substance abuse disorders [1–4]. Therefore, understanding the molecular and cellular mechanisms that underlie the updating of contextual memories is crucial for developing new therapeutic approaches to alleviate persistent and unmalleable contextual fear or compulsive context-induced drug seeking [5–7].

One way to study contextual memories in the laboratory animals is through contextual fear conditioning (CFC) [4]. In CFC, a spatial context, referred to as the conditioned stimulus (CS), is repeatedly paired with a noxious unconditioned stimulus (US), typically a mild shock. Freezing behavior serves as a quantifiable measure of contextual fear memory. With continued exposure to the CS in the absence of the US, freezing behavior generally decreases, and exploratory behavior increases. This process is termed fear extinction and occurs as animals learn over time that the context no longer predicts shocks. For extinction to take place, mice must actively recall and update contextual memories. Therefore, mechanisms must exist in the brain to allow for these processes.

The “classic” neuronal circuit of contextual fear extinction includes medial prefrontal cortex (mPFC), amygdala, and hippocampus [4,8]. However, recent data also support the role of the thalamus in this process [9,10]. In particular, nucleus reuniens (RE), a ventral midline thalamic nucleus, sends axon collaterals to mPFC and the hippocampal CA1 area [11–16], forming a disynaptic link that can coordinate neural activity between the two structures [17–20]. Activity-dependent brain mapping studies have revealed increased cfos expression in the RE following contextual fear extinction learning and recall [21,22]. Activity of RE is synchronized with freezing bouts [23,24], suggesting that activity patterns in the RE are related to suppression of fear responses. Indeed, muscimol-induced inactivation of RE following a weak fear conditioning procedure enhances fear memory consolidation [25]. Moreover, inactivation of the RE prior to extinction training prevents extinction learning, while RE inactivation prior to retrieval impairs retrieval of the extinction memories [21]. Finally, inactivation of the RE also impairs the precision of contextual fear memories and results in fear generalization [21,25,26], a process that requires both the HPC and mPFC [27,28]. Together, these studies suggest that RE may be critical for mPFC-HPC synchrony during the retrieval and updating of contextual memories. This hypothesis is supported by recent studies linking RE→dCA1 activity with recall of fear and extinction memory [20,24].

Here, we sought to determine whether the RE→dCA1 projection plays a role in updating context memories and characterize underlying synaptic processes. First, we used chemogenetic manipulations [29] and conducted ex vivo field recordings in mice to analyze the impact of the RE afferents on synaptic transmission in three strata of the hippocampal CA1 area: the stratum oriens (SO), radiatum (SR), and lacunosum-moleculare (SLM). Secondly, we employed virally mediated labeling of RE afferents in Thy1-GFP mice [30] to analyze the RE buttons and dendritic spines (as a proxy for glutamatergic synapses) in dCA1 during contextual fear memory extinction. This approach was complemented by Serial Block-Face Scanning Electron Microscopy (SBFSEM) [31,32] to analyze synaptic changes induced by contextual fear memory extinction with nano-scale resolution. Finally, using projection-specific chemogenetic manipulation, we tested

the role of the RE→dCA1 projection in the classic contextual fear extinction paradigm, as well as in the extinction of aversive and appetitive memories in a close-to-ecological environment of IntelliCages. Overall, our data support the notion that the RE→dCA1 pathway contributes to updating the value of the context independent of its valence.

Results

Assessment of projections from nucleus reuniens (RE) to dorsal CA1 area (RE→dCA1).

To examine RE axons in dCA1 (RE→dCA1), mice were stereotactically injected into RE with adeno-associated viral vector (isotype 2.1) encoding red fluorescent protein, mCherry, under *camk2a* promoter ($AAV_{2.1}$:camk2a_mCherry) (**Figure 1A**), resulting in mCherry expression in more than 60% of RE cells spreading from Bregma -0.46 mm to -1.5 mm (**Figure 1B**). RE axons visualized by mCherry were visible in the stratum oriens (SO) and lacunosum-moleculare (SLM), but not stratum radiatum (SR), of dCA1 (**Figure 1C-E**). RE buttons were identified as axonal thickenings (> 3 × axon thickness) colocalizing with PSD-95-positive puncta, a marker of excitatory synapses. Density of RE buttons in SLM was slightly lower, and these buttons were much larger, as compared to SO buttons (**Figure 1F-G**).

To test the function of RE→dCA1 projections, mice were stereotactically injected into RE with $AAV_{2.1}$ expressing double-floxed inverted open reading frame (DIO) of Gi-protein-coupled inhibitory DREADD receptor (hM4) and mCherry under human synapsin promoter ($AAV_{2.1}$:hSyn_DIO_hM4_mCherry), and bilaterally into dCA1 with canine adenoviral vector 2 (CAV2) encoding Cre recombinase with GFP under *CMV* promoter (CAV2:CRE_GFP) (**Figure 1H**). This combinatorial manipulation allowed for hM4 expression specifically in RE neurons projecting to dCA1 ($RE^{\rightarrow dCA1}$) (**Figure 1I**). Mice receive i.p. injection of saline or hM4 agonist (CNO, 3 mg/kg), and were sacrificed 30 minutes later. Their brains were sliced and used for recording field excitatory postsynaptic potentials (fEPSP) and fiber volley (FV) in SO, SR and SLM of dCA1, while axons in these strata were stimulated (**Figure 1J-L**). CNO decreased fEPSP in SO and SLM, and FV in SLM. No effect of CNO on these synaptic measures was observed in SR. Hence, our data indicate that RE efficiently regulates excitatory synaptic transmission in SLM and SO.

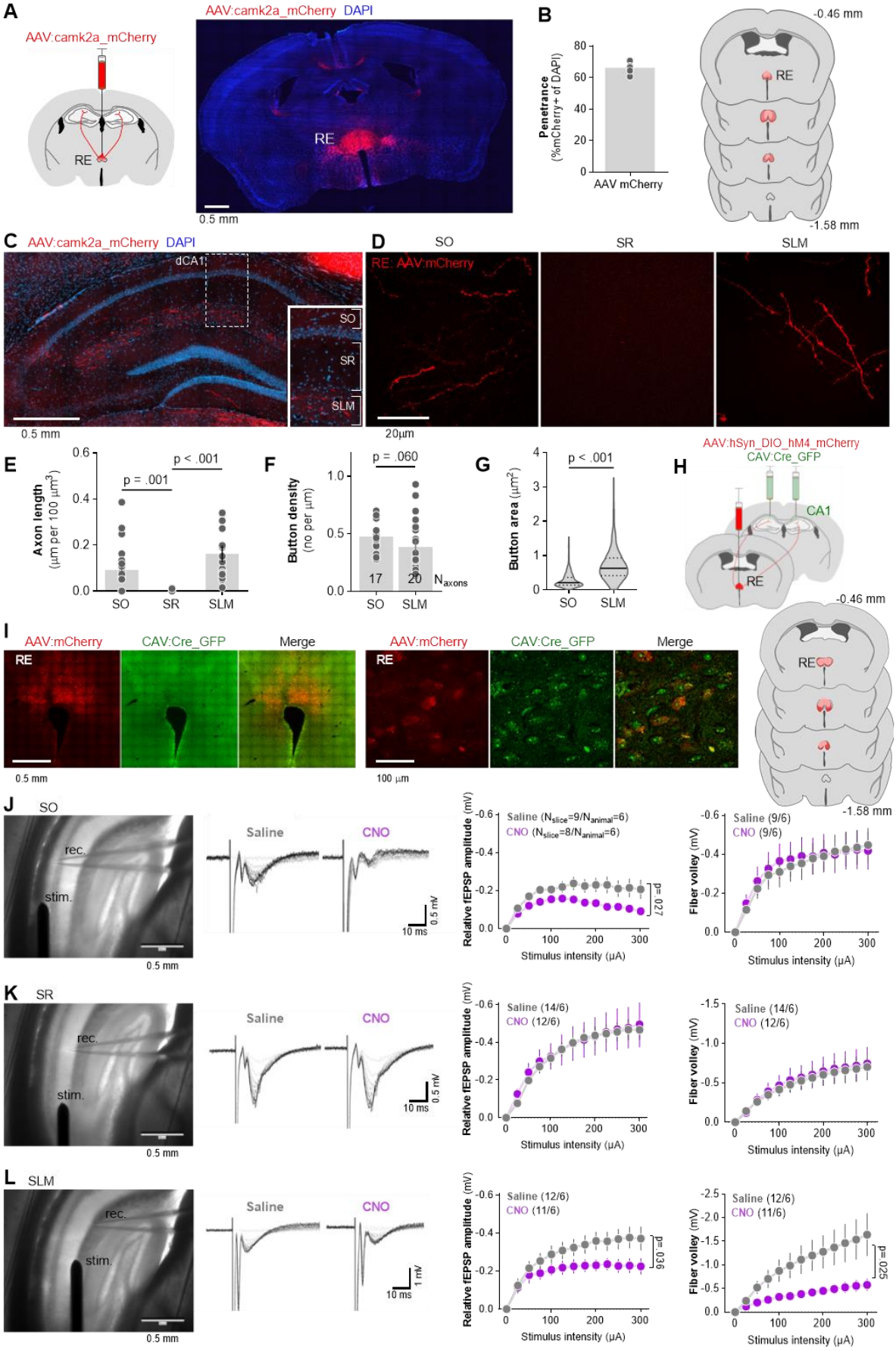

Figure 1. RE regulates synaptic transmission in SO and SLM of dCA1.

(A-B) Experimental schema and virus expression. **(A)** Mice were stereotactically injected into nucleus reuniens (RE) with $AAV_{2.1}$ encoding mCherry. **(B)** A microphotography of mCherry expression in RE, extent of viral expression (pink, minimal; red, maximal) and virus penetrance.

(C-D) Microphotographs showing RE axonal fibers in dorsal hippocampus **(C)** and dCA1 strata **(D)**: stratum oriens (SO), radiatum (SR) and lacunosum-moleculare (SLM). RE buttons were identified as axon thickenings (> 3 × axon thickness) colocalizing with PSD-95-positive puncta.

(E-G) Summary of results showing RE axon length (One-Way ANOVA, Friedman test, $F = 25.29$, $p < 0.001$, $N_{bricks} = 21$ per region), button density (Mann-Whitney test, $U = 108$, $p = 0.060$; SO $N_{axons} = 17$; SLM $N_{axons} = 20$) and button area in dCA1 strata (Mann-Whitney test, $U = 12550$. $p < 0.001$; SO $N_{buttons} = 266$; SLM $N_{buttons} = 282$).

(H-L) The analysis of synaptic responses in dCA1 in mice after chemogenetic inhibition of $RE^{\rightarrow dCA1}$.

(H) Experimental schema. Mice were stereotactically injected with CAV encoding Cre-recombinase with green fluorescent protein (CAV2:Cre_GFP) into dCA1 and with $AAV_{2.1}$ encoding Cre-dependent inhibitory DREADD with mCherry (AAV:DIO_hM4Di_mCherry) into RE, resulting in expression of Cre in neurons projecting to dCA1, and hM4Di in dCA1-projecting neurons of RE ($RE^{\rightarrow dCA1}$). Mice were i.p. injected with saline or CNO (5 mg/kg) and sacrificed 30 minutes later. Their brains were sliced and used for electrophysiological analysis of dCA1 synaptic responses.

(I) Microphotographs showing hM4Di expression in $RE^{\rightarrow dCA1}$, extent of viral expression (pink, minimal; red, maximal) and virus penetrance in mice injected with saline or CNO.

(J-L) Microphotographs of the experimental setups (stim., stimulating electrode; rec., recording electrode), representative fEPSPs traces, summary of data for input–output plots of fEPSP slopes and fiber volley (FV) amplitude recorded in SO (**J**), SR (**K**) and SLM (**L**) in response to increasing intensities of stimulation. CNO decreased fEPSP in SLM (RM ANOVA, $F(1, 24) = 4.95$, $p = 0.036$) and SO ($F(1, 16) = 5.906$, $p = 0.027$) but not in SR ($F(1, 20) = 0.681$, $p = 0.419$). CNO decreased FV amplitudes in SLM (RM two-way ANOVA, $F(1, 17) = 6.057$, $p = 0.025$) but not SO ($F(1, 10) = 0.020$, $p = 0.888$) or SR ($F(1, 25) = 0.042$, $p = 0.839$).

Analysis of dCA1 synapses after contextual fear extinction.

dCA1, RE as well as RE→dCA1 projections have been implicated in the extinction of contextual fear [9,10,20,24]. Moreover, our recent study showed that extinction of contextual fear remodels dendritic spines and results in upregulation of PSD-95 protein specifically in SO and SLM [36]- two CA1 strata where we observed RE axons. Accordingly, we tested whether fear extinction-induced structural plasticity of dCA1 synapses is specific for dendrites innervated by RE. To this end, Thy1-GFP(M) mice (with sparse GFP expression in the excitatory neurons [30] that allows for the analysis of dendritic spine morphology) were stereotactically injected with $AAV_{2.1}$:camk2a_mCherry into RE. Three weeks after the surgery, mice underwent contextual fear conditioning (CFC) with 5 electric shocks in novel context (5US). One group of mice was sacrificed 24 hours later (5US), and the second was re-exposed to the training context for contextual fear extinction (Ext) (**Figure 2A**). At the beginning of the CFC freezing levels were low but increased during the training. At the beginning of the extinction session freezing levels were high, indicating contextual fear memory, and decreased within the session indicating formation of fear extinction memory (**Figure 2A**) [36]. Post-training analysis of the brain sections showed that mCherry was expressed in RE, the levels of AAV transduction did not differ between the experimental groups and was observed in over 60% of RE cells (**Figure 2B**). RE buttons

were identified in SO and SLM of dCA1 as mCherry-positive axonal thickenings collocalizing with PSD-95-positive puncta. We distinguished dCA1 dendrites innervated by RE (RE+ dendrite: colocalizing with RE buttons and PSD-95 puncta), and dCA1 dendrites that did not colocalize with RE buttons within the analyzed tissue brick (RE- dendrite) (**Figure 2C**).

There were no significant differences between the experimental groups in RE button density and size in SO (**Figure 2D**). We found, however, that in SLM the Ext mice had significantly bigger RE buttons than 5US animals. The density of RE buttons was not affected by the training in this region (**Figure 2E**).

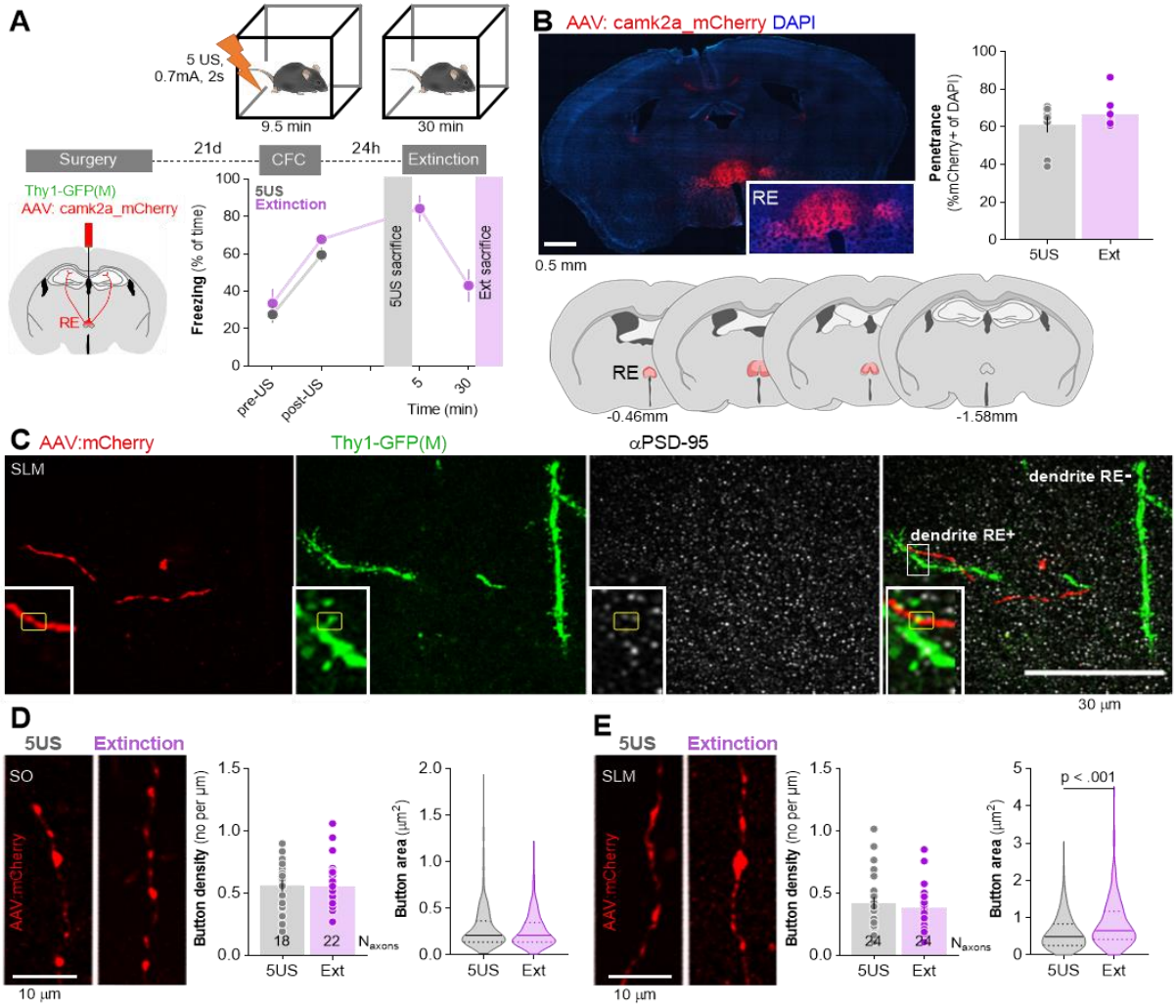

Figure 2. Extinction of contextual fear remodels RE buttons in SLM.

(A) Experimental timeline and summary of data showing freezing levels during CFC and fear extinction session. After injection of $AAV_{2.1}$ encoding mCherry into RE, Thy1-GFP(M) mice underwent CFC and were sacrificed 24 hours later (5US) or underwent fear extinction session and were sacrificed after the session (Ext). **(B)** mCherry expression analysis in RE. **(Left)** Confocal scan of RE with local expression of mCherry. **(Right)** Penetrance of mCherry in 5US and Ext mice.

(C-E) RE axons analysis in SO and SLM of Thy1-GFP(M) mice. **(C)** Representative high-magnification scans in SLM showing RE axons (red), dendritic spines (green), and a marker of the excitatory synapses, PSD-95 protein (gray). RE buttons were identified as axon thickenings (> 3 × axon thickness) collocalizing with PSD-95-positive puncta. dCA1 dendrites colocalizing with RE axon (dendrite RE+), and dCA1 dendrites not co-

localizing with RE axon (dendrite RE-) were identified within tissue bricks (67.7 × 67.7 × 5.4 μm; from z-stack of 20 microphotographs).

(D) Representative images of RE axons in SO **(Left)** and summary of data showing button density (unpaired t-test, $t(38) = 0.102$; $p = 0.918$)**,** and button area (Mann Whiteny test, $U = 38365$; $p = 0.193$) **(Right)**. 5US $N_{buttons}$= 203, $N_{animals}$= 6; Extinction $N_{buttons}$= 400, $N_{animals}$= 6.

(E) Representative images of RE axons in SLM **(Left)** and data analyzing of button density (unpaired t-test, $t(46) = 0.642$; $p = 0.523$) and button area (Mann Whiteny test, $U = 29409$; $p < 0.001$) **(Right)**. 5US $N_{buttons}$= 272, $N_{animals}$= 6; Extinction $N_{buttons}$= 291, $N_{animals}$= 6.

Moreover, the Ext group had less dendritic spines in SO as compared to 5US animals (**Figure 3A**) and this change was specific for the RE- dendrites. The remaining dendritic spines did not differ in median area, but they contained more PSD-95 (measured as mean gray value of PSD-95 signal per dendritic spine), suggesting enlargement of synapses. Again, the change of PSD-95 puncta was specific for the RE- dendrites (**Figure 3A**). In SR, we did not observe any significant differences in density and size of dendritic spines or PSD-95 levels between the Ext and 5US groups (**Figure 3B**). Interestingly, in SLM the median dendritic spine area and PSD-95 expression per dendritic spine were higher in the Ext group as compared to 5US animals, and these differences were specific for the RE+ dendrites. We did not observe any changes in dendritic spines density in SLM after extinction of contextual fear (**Figure 3C**).

To test whether the observed changes of synaptic buttons and dendritic spines in SLM were specific for contextual fear extinction, we conducted a control experiment with Thy1-GFP mice expressing mCherry in RE neurons (**Figure 4A**). The animals were exposed to the novel experimental context without electric shocks and were sacrificed 24 hours later (Ctx) or immediately after re-exposure to the same context for 30 minutes (Ctx-Ctx). The mice showed low levels of freezing both during the first and second exposure to the experimental context, indicating no fear memory. We observed no differences in density and size of RE buttons (**Figure 4B-C**) and dendritic spines (**Figure 4D-E**) in SLM between the experimental groups.

Hence, our data indicates that contextual fear extinction specifically remodels RE→dCA1 synapses in SLM. This process is characterized by global growth of RE→SLM buttons and dendritic spines located on RE+ dendrites, as well as increased expression of synaptic scaffold protein, PSD-95, on these spines. Such changes are not observed in the animals exposed to the novel context without US, supporting the role of SLM structural plasticity in contextual fear extinction rather than novel context exposure. At the same time, contextual fear extinction-induced structural plasticity of dendritic spines in SO was observed on the dendrites that did not colocalize with RE axons.

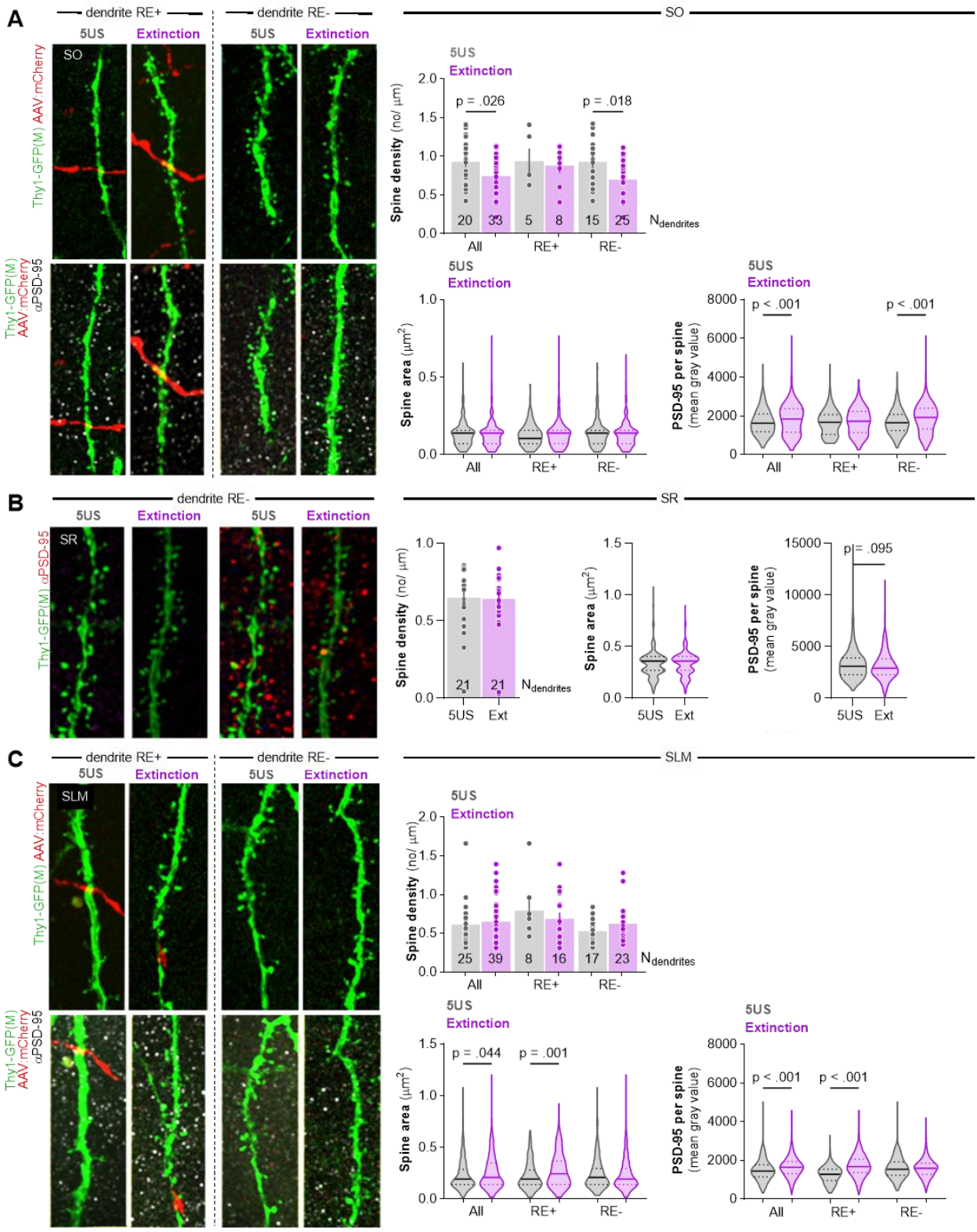

Figure 3. Extinction of contextual fear remodels SLM dendritic spines on RE+ dendrites.

Thy1-GFP mice were injected with $AAV_{2.1}$:camk2a_mCherry into RE and 21 days later they underwent CFC and were sacrificed 24 hours later (5US, n = 6), or underwent contextual fear extinction session and were sacrificed after the session (Extinction, n = 6) (see Figure 2A).

(A) Analysis of dendritic spines in SO. **(left)** Representative high-resolution images of RE axons (red), RE+ and RE- dendritic fragments (green), and PSD-95 immunostaining (gray) in 5US and Ext groups. **(right)** Summary of data showing density of dendritic spines (One-way ANOVA with LSD tests for planned

comparisons, F = 3,619; p = 0.034), dendritic spine area (Kruskal-Wallis test, U = 3.62; p = 0.605) and PSD-95 expression per dendritic spine (Kruskal-Wallis test with Dunn's *post hoc* tests for planned comparisons, U =53.9; p < 0.001). 5US RE+: N_{spines}= 81; 5US RE-: N_{spines}= 310; Extinction RE+: N_{spines}= 274; Extinction RE-: N_{spines}= 800.

(B) Analysis of dendritic spines in SR. Representative high-resolution images of RE- dendritic fragments (green), and PSD-95 immunostaining (red). Summary of data showing density of dendritic spines (t-test, t(40) = 0.084, p = 0.93), dendritic spine area (Mann-Whitney test; U = 213, p = 0.863) and PSD-95 expression per dendritic spine (Mann-Whitney test; U = 217833, p = 0.095). 5US N_{spines}= 471; Extinction N_{spines}= 716.

(C) Analysis of dendritic spines in SLM. Representative high-resolution images of RE axons (red), RE+ and RE- dendritic fragments (green), and PSD-95 immunostaining (gray). Summary of data showing density of dendritic spines (One-way ANOVA, effect of group: F(5, 122) = 1.36, p = 0.243), dendritic spine area (Kruskal-Wallis test with Dunn's *post hoc* tests, U = 23.6; p < 0.001) and PSD-95 expression per dendritic spine (Kruskal-Wallis test with Dunn's *post hoc* tests, U = 148; p < 0.001). 5US RE+: N_{spines}= 212; 5US RE-: N_{spines}= 310; Extinction RE+: N_{spines}= 385; Extinction RE-: N_{spines}= 546.

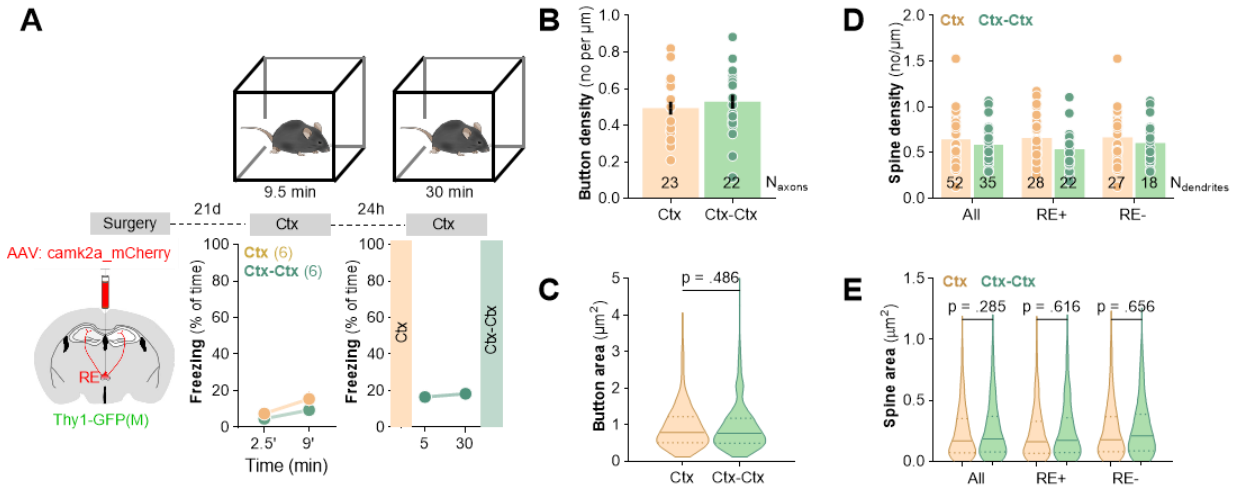

Figure 4. Novel context exposure remodels neither axonal buttons nor dendritic spines in SLM.

(A) Experimental timeline and summary of data showing mice activity levels during novel context exposure. Thy1-GFP mice were stereotactically injected with $AAV_{2.1}$:camk2a_mCherry into RE and 21 days later they were exposed to a novel context. Mice were sacrificed 24 hours after novel context exposure (Ctx) or they were re-exposed to the context and sacrificed immediately afterwards (Ctx-Ctx).

(B-C) Morphological analysis of RE axons in SLM. **B)** Summary of data showing button density (unpaired t-test, t(43) = 0.682, p = 0.43) and **(C)** button area (Mann Whiteny test, U = 2745; p = 0.48). Ctx $N_{buttons}$ = 230, $N_{animals}$= 6; Ctx-Ctx $N_{buttons}$= 239, $N_{animals}$= 6.

(D-E) Analysis of dendritic spines in SLM. **(D)** Summary of data showing spine density (Mixed- effect Model, Sidak's multiple comparison test, F(1,93) = 3.18, p = 0.078) and **(E)** spine area (Kruskal-Wallis tests). Ctx RE+: N_{spines}= 569; Ctx RE-: N_{spines}= 436; Ctx-Ctx RE+: N_{spines}= 413; Ctx-Ctx RE- N_{spines}= 318. For A, B and D, data are presented as means and SEM. For C and E, data are presented as medians and IQR.

Nano-scale resolution analysis of SLM synapses after contextual fear extinction

To confirm whether contextual fear extinction induces growth of SLM synapses we used Serial Block-Face Scanning Electron Microscopy (SBFSEM). This approach lacked specificity for RE→SLM projections, however, it allowed us to reconstruct SLM dendritic spines with nano-scale resolution, as well as image and analyze postsynaptic densities (PSDs), representing post-synaptic part of the excitatory synapse (**Figure 5A-B**). In total, we reconstructed 311 dendritic spines with PSDs from the brains of naïve mice (n = 4), 199 from the brains of the mice sacrificed 24 hours after CFC (5US, n = 4) and 161 of the mice sacrificed after extinction session (Ext, n = 4).

We found that dendritic spine density did not differ between the experimental groups (**Figure 5C**). However, dendritic spine volume, PSDs volume and surface area were higher in the Ext group as compared to Naive and 5US animals (**Figure 5D-F**). Moreover, we analyzed the correlation between dendritic spine volume, PSD volume and PSD surface area. These parameters were tightly correlated in all experimental groups (**Figure 5G-H**). However, the lines describing these correlations in the Ext animals were slightly moved upwards, as compared to the 5US group, indicating that during the extinction session PSDs increased in size more than dendritic spines. Hence, SBFSEM analysis confirmed that contextual fear extinction results in strengthening of SLM excitatory synapses.

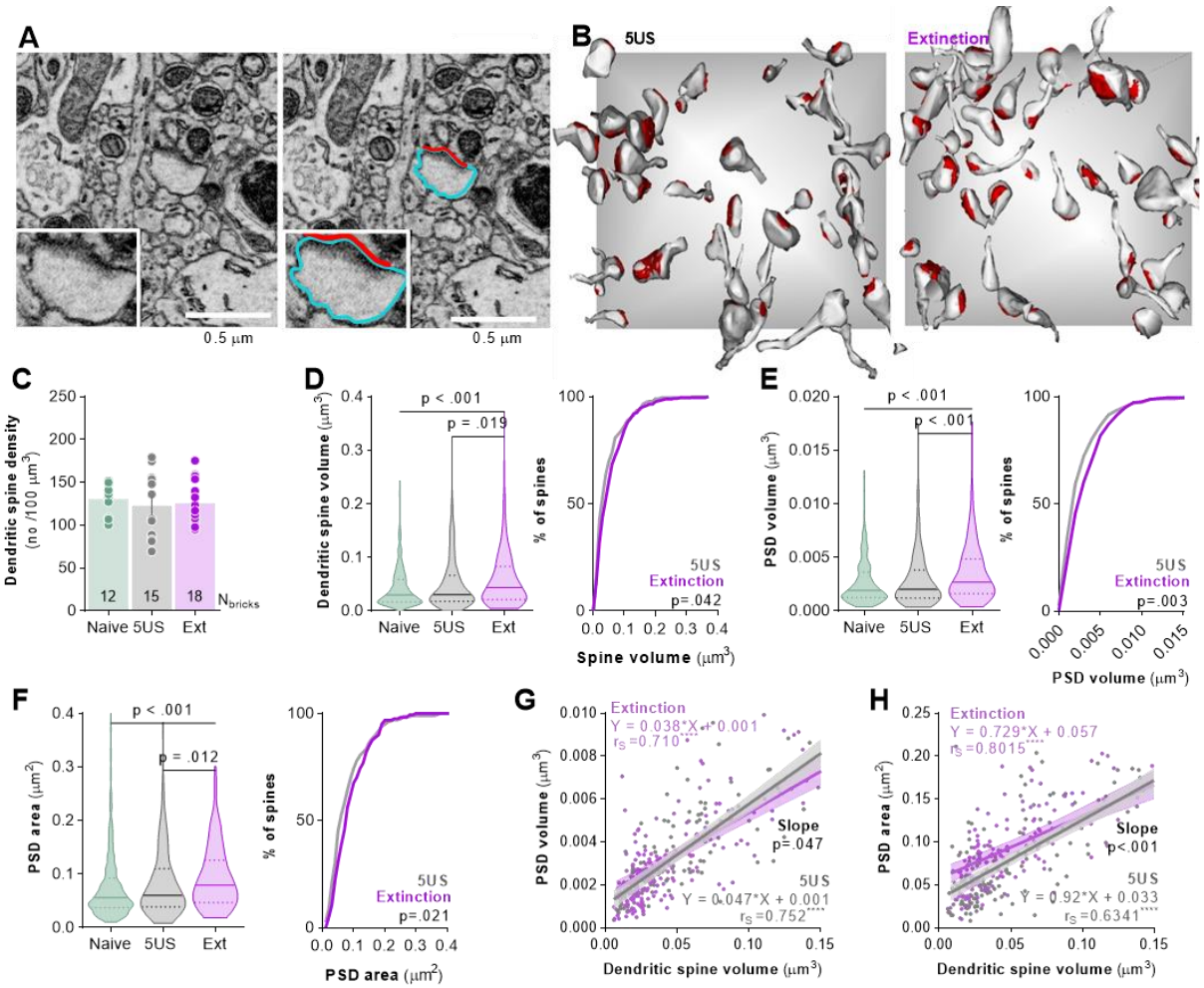

Figure 5. **Contextual fear extinction remodels synapses in SLM.**
Mice underwent CFC and were sacrificed 24 hours later (5US, n = 5) or after re-exposure to the training context without electric shocks (Ext, n = 5). Naive mice were used as a control (n = 4).

(A-B) The principles for SBFSEM analysis of dendritic spines and PSDs in SLM. **(A)** Tracing of a dendritic spine and PSD. A representative trace of a dendritic spine (blue), PSD surface area (red) and volume (yellow). **(B)** Exemplary reconstructions of dendritic spines and their PSDs from SBFSEM scans in SLM for the 5US and Ext groups. Dendritic spines and PSDs were reconstructed and analyzed in tissue bricks (6 × 6 × 2.5 µm). The gray background square is x = 6 × y = 6 µm.

(C-H) Summary of SBFSEM data: **(C)** density of dendritic spines (Kruskal-Wallis test, U = 0.27, p = 0.870); **(D)** volume of dendritic spines (Kruskal-Wallis test with Dunn's *post hoc* tests, U = 13.2, p < 0.001; Kolmogorov-Smirnov D = 0.125, p = 0.042); **(E)** volume of PSDs (Kruskal-Wallis test with Dunn's *post hoc* tests, U = 21.4, p < 0.001; Kolmogorov-Smirnov D = 0.160, p = 0.003); **(F)** surface area of PSDs (Kruskal-Wallis test with Dunn's *post hoc* tests, U = 17.9, p < 0.001; Kolmogorov-Smirnov D = 0.160, p = 0.021); and **(H)** correlation of dendritic spine volume and PSD surface area (r_s, Spearman correlation r). For C, each dot represents one tissue brick; for D-F (left), medians ± IQR are shown; for G and H each dot represents one dendritic spine.

Functional analysis of RE→dCA1 pathway during contextual fear extinction.

To test whether RE→dCA1 pathway affects contextual fear extinction, C57BL/6J mice were injected with $AAV_{2.1}$:DIO_hM4 into RE and with CAV2:Cre into dCA1(**Figure 6A**) resulting in hM4 expression in the $RE^{\rightarrow dCA1}$ neurons (**Figure 6B**)**.** Three weeks post-surgery and viral infection, mice underwent CFC, followed by a contextual fear extinction session. Mice were injected with CNO (i.p., 3 mg/ kg) or Saline 30 minutes prior to the Extinction (**Figure 6A**). The freezing levels increased within the conditioning session (pre- vs post-US) and did not differ between the drug groups. During the Extinction session, the mice from two experimental groups had similar freezing levels at the beginning of the session and decreased freezing during the session, indicating no impairment of fear memory recall and successful within-session fear extinction. Consolidation of long-term fear extinction memory was tested 24 hours after the Extinction session in the same context (Test). Mice from the CNO group had higher levels of freezing as compared to the Saline animals, suggesting impaired long-term fear extinction memory (**Figure 6A**).

As RE was linked with fear generalization [26] we also tested the role of RE→dCA1 pathway in the recognition of the training context. The second cohort of mice underwent CFC, followed by a fear extinction session (Extinction 1). Next, we tested short-term (Test 1, 2 hr post Extinction 1) and long-term fear extinction memory (Extinction 2, 24 hr post Extinction 1) as well as fear generalization in the context B (CtxB, 2 hr post Test 2). Mice were injected with CNO or Saline 30 minutes prior to the Extinction 1 and Test 2 (**Figure 6C**). As for the first cohort, we did not observe any differences in the freezing levels between Saline and CNO groups during the CFC and Extinction 1. Mice in both groups successfully formed contextual fear memory, as indicated by high levels of freezing in the training context at the beginning of the Extinction 1, and decreased freezing level within this session. However, the CNO group, as compared to the Saline animals, showed higher freezing levels both during a short-term (Test 1) and long-term fear extinction memory test (Extinction 2). They showed, however, no difference in freezing levels in the CtxB (**Figure 6C**). Hence, our results indicate that $RE^{\rightarrow dCA1}$ regulates formation of short- and long-term contextual fear extinction memory but not recognition of the training context.

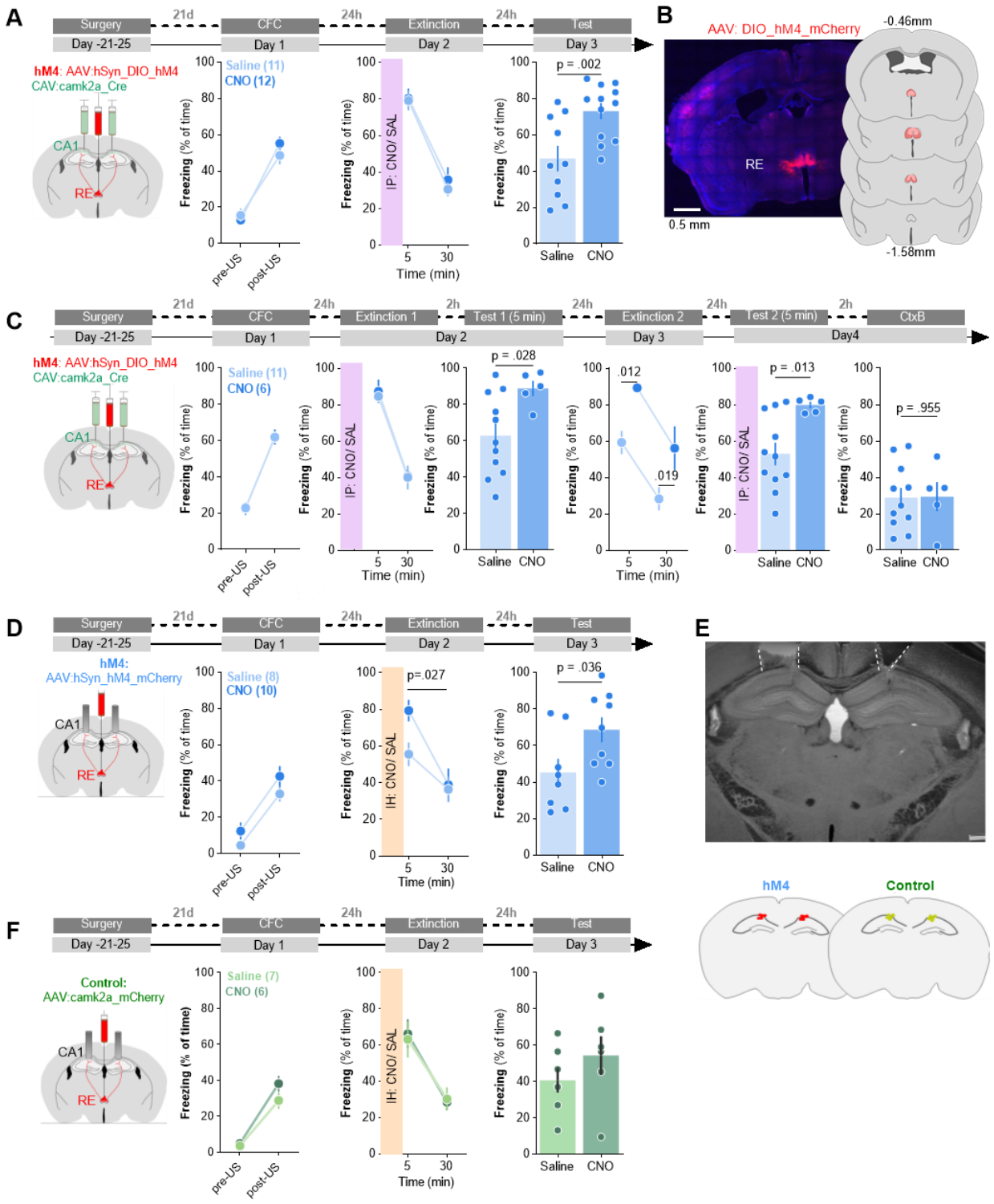

Figure 6. Chemogenetic inhibition of RE→dCA1 impairs extinction of contextual fear memory.

(A-B) Experimental timeline and summary of data for freezing levels during the training. After stereotactic injection of $AAV_{2.1}$:DIO_hM4_mCherry (DIO_hM4) into RE and CAV:Cre_GFP into dCA1 mice underwent CFC (Training: RM ANOVA with Fisher's LSD *post hoc* test, effect of time: $F(1, 21) = 446$, $p < 0.001$; effect of CNO: $F(1, 21) = 0.165$, $p = 0.689$; time × CNO interaction: $F(1, 21) = 6.64$, $p = 0.018$), fear extinction session (Extinction: RM ANOVA with Šidak's *post hoc* test, effect of time: $F(1, 21) = 95.55$, $p < 0.001$; effect of CNO: $F(1, 21) = 0.259$, $p = 0.616$; time × CNO interaction: $F(1, 21) = 0.1740$, $p = 0.681$) and fear extinction test

(Test: unpaired t-test: t(20) = 3.26, p = 0.002). **(B)** Representative microphotographs of hM4 expression in RE and the extent of viral expression (pink, minimal; red, maximal). **(C)** Experimental timeline and summary of data for freezing levels during the training. After stereotactic injection of DIO_hM4 into RE and CAV:Cre_GFP into dCA1 mice underwent CFC (Training: RM ANOVA with Šidak's *post hoc* test, effect of time: F(1, 14) = 218, p < 0.001; effect of CNO: F(1, 14) = 0.001, p = 0.974; time × CNO interaction: F(1, 14) = 0.010, p = 0.919), fear extinction session (Extinction: RM ANOVA with Šidak's *post hoc* test, effect of time: F(1, 14) = 45.5, p < 0.001; effect of CNO: F(1, 14) = 0.121, p = 0.73; time × CNO interaction: F(1, 14) = 0.020, p = 0.89), short-term extinction memory test (STM: t-test: t(14) = 2.45, p = 0.028), long-term extinction memory test (LTM: RM ANOVA with Šidak's *post hoc* test, effect of time: F(1, 14) = 23.1, p < 0.001; effect of CNO: F(1, 14) = 10.5, p = 0.006; time × CNO interaction: F(1, 14) = 0.028, p = 0.87) and exposure to the context B (CtxB: unpaired t-test: t(14) = 0.057, p = 0.955). **(D-E)** Experimental timeline and summary of data for freezing levels during the training. Mice were stereotactically injected into RE with $AAV_{2.1}$ encoding hM4Di and a cannula placed into dCA1. Next, they underwent CFC (Training: RM ANOVA with Šidak's *post hoc* tests, effect of time: F(1, 12) = 146, p < 0.001; effect of CNO: F(1, 12) = 1.60. p = 0.23; time × CNO interaction: F(1, 12) = 0.12, p = 0.72), contextual fear extinction session (Extinction: RM ANOVA with Šidak's *post hoc* test, effect of time: F(1, 15) = 36, p < 0.001; effect of CNO: F(1, 15) = 2.14, p = 0.16; time × CNO interaction: F(1, 15) = 4.59, p = 0.49) and long-term fear extinction memory test (unpaired t-test, t(15) = 2.30. p = 0.036). **(E)** Microphotography of cannula placement. **(F)** Experimental timeline and summary of data for freezing levels during the training. Mice were stereotactically injected into RE with AAV2.1 encoding mCherry and cannula were placed into dCA1. After surgery they underwent CFC (Training: RM ANOVA with Šidak's *post hoc* tests, effect of time: F(1, 10) = 84.3, p < 0.001; effect of CNO: F(1, 10) = 2.18, p = 0.17; time × CNO interaction: F(1, 10) = 1.61, p = 0.23), fear extinction session (RM ANOVA with Šidak's *post hoc* test, effect of time: F(1, 11) = 25.8, p < 0.001; effect of CNO: F(1, 11) = 0.006, p = 0.93; time × CNO interaction: F(1, 11) = 0.12, p = 0.72) and memory test (unpaired t-test, t(11) = 1.12, p = 0.28).

Since $RE^{\rightarrow dCA1}$ neurons likely innervate also other brain areas [11], in the following experiment we tested whether specific inhibition of RE→dCA1 axons affects contextual fear extinction. Mice were stereotactically injected into RE with $AAV_{2.1}$:hSyn_hM4_mCherry, or $AAV_{2.1}$:camk2a_mCherry as a control (**Figure 6D-F**). Next, we implanted a cannula into dCA1 to deliver Saline or CNO locally. Twenty one days after the surgery and virus expression, mice underwent CFC, followed by an Extinction session and Test (**Figure 6D-F**). During the training mice had a low level of freezing before US (pre-US) (**Figure 6D**). Freezing levels increased across a CFC session (post-US) and did not differ between the drug groups. Twenty four hours later mice received bilateral intra-hippocampal injection of CNO (3 μM) or Saline and were re-exposed to the training context (Extinction). In the hM4 virus group, mice injected with CNO showed higher freezing during the first 5 minutes of Extinction, compared to the mice injected with Saline. During Extinction the freezing level decreased and did not differ between the groups at the end of the session. However, when extinction memory was tested (Test) the hM4 mice injected with CNO had higher levels of freezing compared to the mice injected with Saline. Levels of freezing in mCherry CNO and Saline groups differed neither during the Training, nor during Extinction and Test (**Figure 6F**).

Overall, these results indicate that transient inhibition of RE→dCA1 has a long-lasting effect and impairs extinction of contextual fear. We have also observed that it enhances contextual fear recall but has no effect on contextual fear memory generalization. Interestingly, in the Saline groups with cannulae the freezing levels were lower as compared to the control groups in the experiments without cannulae (58-62% vs 68-83%), suggesting that cannula implantation impaired memory formation, possibly due to damage to the hippocampus. Hence, inhibition of RE→dCA1 may enhance contextual fear recall only when the memory trace is weak.

The impact of RE on contextual fear extinction-induced synaptic plasticity in dCA1.

To test whether RE affects contextual fear extinction-induced synaptic plasticity in dCA1, C57BL/6J mice were injected with hM4 or Control virus into RE (**Figure 6A-C**). Three weeks post-surgery and viral infection, mice underwent CFC, followed by a contextual fear extinction session. Mice were injected with CNO (i.p., 3 mg/ kg) or Saline 30 minutes prior to the Extinction (**Figure 6A**). The freezing levels increased within the conditioning session (pre- vs post-US) and did not differ between the experimental groups. During the Extinction session, the mice from four experimental groups had similar freezing levels at the beginning of the session and decreased freezing during the session, indicating no impairment of fear memory recall and successful within-session fear extinction. Mice were sacrificed immediately after Extinction and their brains were sliced. We analyzed the changes of PSD-95 protein levels in three dCA1 strata (as a proxy for remodeling of excitatory synapses) using fluorescent immunostaining.

PSD-95 levels were significantly lower in SR and SLM in the hM4 group treated with CNO, as compared to the Control group treated with CNO and the hM4 group treated with Saline. Moreover, PSD-95 levels were significantly lower in all strata in the hM4 group treated with CNO, as compared to the Control group treated with Saline (**Figure 6D**). Hence, chemogenetic inhibition of RE during contextual fear extinction affected training-induced molecular changes of the excitatory synapses in dCA1.

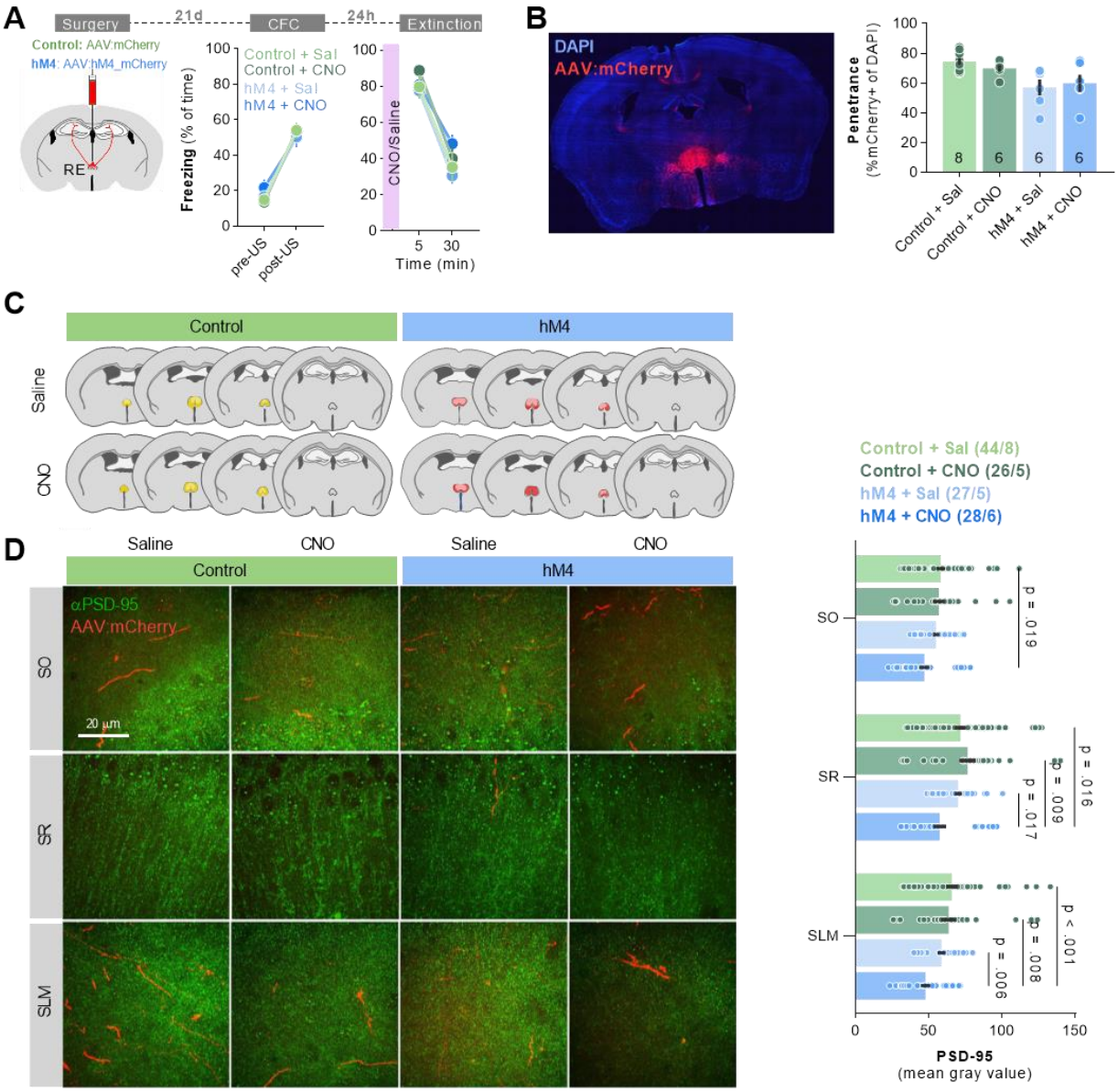

Figure 7. RE regulates dCA1 excitatory synapses during contextual fear extinction.

(A) Experimental timeline and summary of data showing freezing levels during CFC and contextual fear extinction. After injection of $AAV_{2.1}$ encoding mCherry (Control) or hM4 into RE, mice underwent CFC and fear extinction session. Mice were injected with CNO or Saline 30 minutes before Extinction and were sacrificed immediately after the session. The dCA1 brain slices with visible RE axons were used for PSD-95 immunostaining.

(B-C) AAVs expression analysis in RE. **(Left)** Confocal scan of RE with local expression of mCherry. **(Right)** Penetrance of mCherry in experimental groups. **(C)** The extent of viral expression.

(D) Representative images of PSD-95 immunofluorescent staining and RE axons (red) in 3 strata of dCA1 **(Left)** and data analysis (three-way RM ANOVA with *post hoc* LSD test for planned comparisons, effect of virus: $F(1, 21) = 8.58$, $p = 0.008$; effect of CNO: $F(1, 21) = 0.566$, $p = 0.460$; virus × CNO interaction: $F(1, 21) = 7.72$, $p = 0.011$). The numbers of the analyzed sections and animals are indicated in the legend.

Functional analysis of RE→dCA1 pathway during place avoidance and preference training and extinction in close-to-ecologic conditions.

We next investigated whether the RE→dCA1 pathway contributes to updating context value in complex, close-to-ecologic conditions. C57BL/6J mice were bilaterally injected with CAV2:Cre_GFP into dCA1 and with $AAV_{2.1}$:hSyn_DIO_hM4_mCherry into RE, and three weeks later they were trained in the social context of IntelliCages (**Figure 8A**). The animals underwent place preference training (sucrose in one cage corner) followed by preference extinction (water in both active cage corners), place avoidance training (quinine in one corner) and avoidance extinction (water in both active cage corners) (**Figure 8A**). Thirty minutes prior to the place preference and place avoidance trainings mice received i.p. injection of CNO (3 mg/kg) or saline. Furthermore, mice in the CNO cage had CNO dissolved in drinking water to consume approx. 3 g/kg/day. We did not observe any significant differences in general activity (measured as total visits in cage corners and liquid consumption) between the mice in the CNO and Water cages at any stage of the training (**Supplementary Figure 1**). However, all mice performed more visits and licks in the reward corner during place preference training, as compared to all other periods of the experiment. Post-training analysis of the brain sections confirmed hM4 expression in RE (**Figure 8B**).

During the place preference training the frequency of visits to the sucrose corner increased in both experimental groups, and no effect of CNO was observed (**Figure 8C**). During the preference extinction, the frequency of visits to the sucrose corner decreased in both experimental groups. However, the change of corner preference was smaller in the CNO mice, as compared to the Water group (**Figure 8D**). During the first 6 hours of place avoidance training, the frequency of visits to the quinine corner decreased only in the Saline group, and a significant effect of CNO was observed (**Figure 8E**). During the avoidance extinction, the frequency of visits to the quinine corner significantly increased only in the Water group. Hence the change of corner preference was smaller in the CNO mice, as compared to the Water group (**Figure 8F**). Altogether, our data indicates that inhibition of the RE→dCA1 pathway significantly affects the frequency of correct choices during place avoidance training as well as extinction of place preference and avoidance. It has no effect on spatial choice during place preference training.

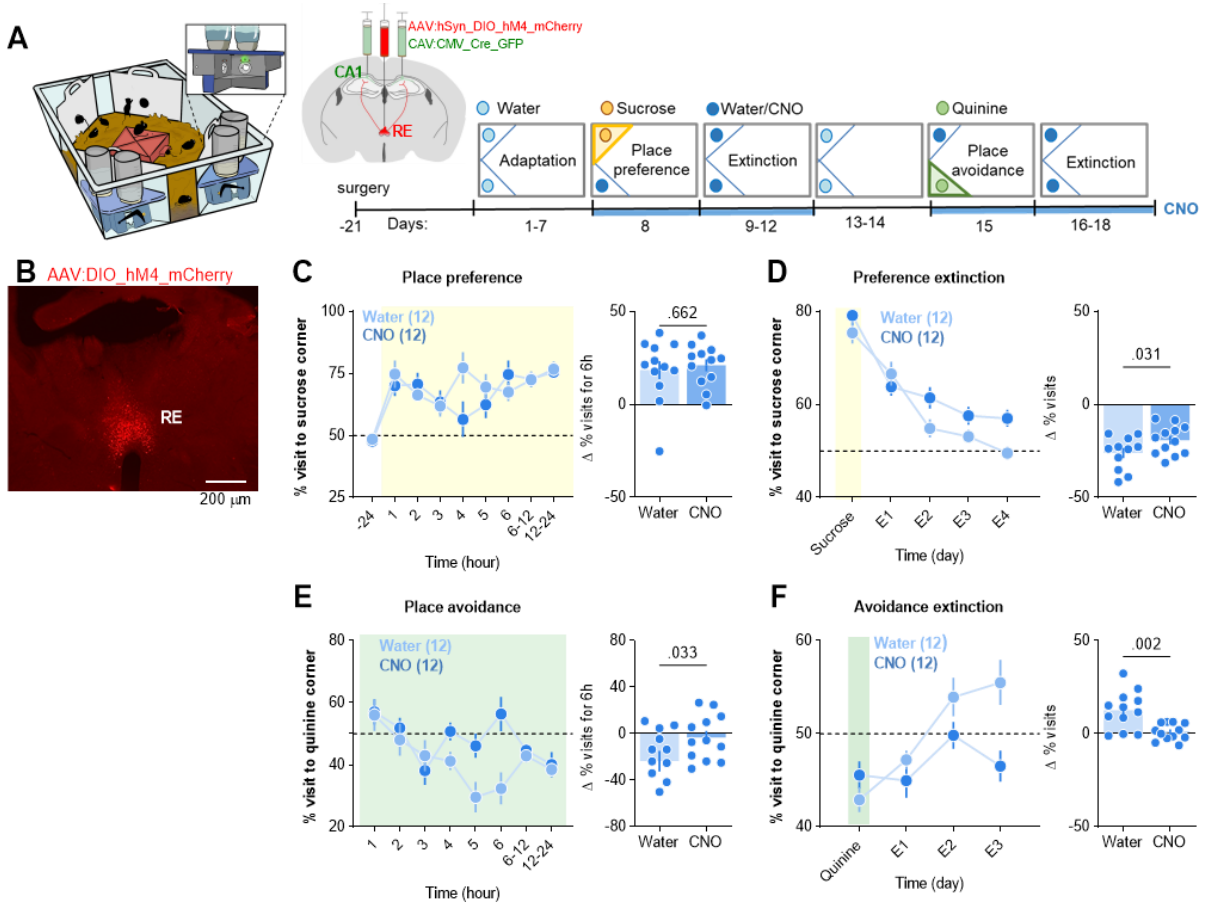

Figure 8. Chemogenetic inhibition of RE→dCA1 impairs extinction of place avoidance and preference in close-to-ecologic conditions.

(A) A schematic view of IntelliCage and experimental timeline. Mice had stereotactic injection of $AAV_{2.1}$: hSyn_DIO_hM4_mCherry in RE and CAV_2: camk2a_Cre_GFP in dCA1. Three weeks after the surgery and virus expression, they were trained in IntelliCages - place preference training was followed by preference extinction, place avoidance and avoidance extinction. During training and extinction sessions CNO mice had CNO dissolved in drinking water.

(B) Representative microphotographs of hM4 expression in RE and the extent of viral expression (pink, minimal; red, maximal).

(C-D) Summary of data for place preference and preference extinction. **(C)** Frequency of visit to sucrose corner (RM ANOVA, effect of time: $F(4.58, 97.4) = 8.18$, $p < 0.001$; effect of CNO: $F(1, 22) = 0.634$, $p = 0.434$; time × CNO interaction: $F(8,170) = 1.90$. $p = 0.062$) and change of preference during 6 hours of training (right, t-test). **(D)** Frequency of visit to ex-sucrose corner (RM ANOVA, effect of time: $F(2.28, 50.2) = 67.25$, $p < 0.0001$; effect of CNO: $F(1, 22) = 1.31$, $p = 0.264$; time × CNO interaction: $F(4, 88) = 2.51$, $p = 0.047$) and change of preference during 4 days of training (right, t-test).

(E-F) Summary of data for place avoidance and avoidance extinction. **(E)** Frequency of visit to quinine corner (RM ANOVA, effect of time: $F(4,26, 85,2) = 5.56$, $p < 0.0001$; effect of CNO: $F(1, 22) = 5.11$, $p = 0.034$; time × CNO interaction: $F(7, 140) = 1.69$, $p = 0.117$) and change of preference during 6 hours of training (right, t-test). **(F)** Frequency of visit to ex-quinine corner (RM ANOVA, effect of time: $F(2,24, 49,2) = 15.4$, $p = 0.001$;

effect of CNO: $F(1, 22) = 3.17$, $p = 0.089$; time × CNO interaction: $F(3, 66) = 6.41$, $p < 0.001$) and change of preference during 3 days of training (right; t-test).

Discussion

Understanding the neuronal circuits that mediate the updating of contextual information is crucial for improving therapeutics for trauma- and reward-related disorders, such as post-traumatic stress disorder or drug use disorders. Previous research has indicated that the RE and dCA1 are necessary for the formation and retrieval of fear extinction memories. However, the function of the projections between these regions is less understood. In this study, we confirmed that RE axons innervate dCA1 neurons and chemogenetic inhibition of RE impairs excitatory synaptic transmission in SO and SLM. Moreover, we discovered that in the SLM contextual fear memory extinction remodels dendritic spines and upregulates the levels of synaptic scaffold, PSD-95, on dendrites innervated by RE. Chemogenetic inhibition of RE blocked the contextual fear extinction-induced expression of PSD-95 in dCA1. Finally, chemogenetic inhibition of the RE→dCA1 pathway impaired the consolidation of contextual fear extinction memory, as well as the extinction of place preference and avoidance in conditions close to ecologic. In summary, our observations support a framework in which the RE→dCA1 pathway actively regulates training-induced synaptic plasticity in dCA1, promoting the updating of context value.

RE projects to the hippocampal formation and forms asymmetric synapses with dendritic spines and dendrites, suggesting innervation of excitatory synapses on both excitatory and aspiny inhibitory neurons [16,37–39]. This conclusion was confirmed by the electrophysiological studies showing that RE modulates function of the pyramidal cells by monosynaptic excitatory and polysynaptic inhibitory mechanisms [15,38]. Here, we observed RE buttons in close apposition to dCA1 dendritic spines with PSD-95-positive puncta, confirming innervation of pyramidal neurons via excitatory synapses, and the RE axons were found both in SO and SLM of dCA1, with the later having much bigger buttons. Furthermore, we recorded fEPSPs in dCA1 while chemogenetically inhibiting RE axons. This manipulation decreased fEPSPs both in SO and SLM, and had no effect on this parameter in SR. Hence, our data supports the notion that RE activity increases excitatory synaptic transmission in SO and SLM. Since RE projections were described so far only in SLM, the observation of RE axons in SO is surprising. However, closer inspection of the published confocal microphotographs of dCA1 after fluorescent labeling of RE axons suggests that RE→SO projections were labeled by other groups as well [24].

Both formation [40–43] and extinction of contextual fear memories [44–46] involve synaptic plasticity in dCA1. In particular, our previous work has demonstrated that contextual fear extinction induces remodeling of excitatory synapses in dCA1 [36]. This synaptic plasticity is stratum-specific and requires phosphorylation of PSD-95 at serine 73. We also demonstrated that phosphorylation of PSD-95 at serine 73 is required for contextual fear extinction. Thus, PSD-95-dependent synaptic plasticity is an important step in the regulation of the dCA1 circuit during contextual fear extinction. Here, we confirmed the earlier observations and specified that extinction-induced changes of dendritic spines and PSD-95 are observed on RE+ dendrites in SLM, and RE- dendrites in SO. This observation is complemented by the analysis of RE buttons showing the increased median size of RE buttons in SLM, but not SO, after contextual fear extinction sessions. We also found that RE inhibition blocks the contextual fear extinction-induced expression of PSD-95 in all three strata of CA1, and chemogenetic inhibition of RE→dCA1 blocks formation of short- and long-term contextual fear extinction

memory. Thus our data indicate that RE projections regulate dCA1 synaptic plasticity that is necessary for consolidation of contextual fear extinction memory.

The former studies demonstrated the role of the RE in fear memory encoding, retrieval, extinction and generalization [21,26,47–50]. Furthermore, recent work has demonstrated the role of the RE→dCA1 pathway in extinction of contextual fear and recall of contextual fear extinction [20,24]. In agreement with these findings, inhibition of the $RE^{\rightarrow CA1}$ neurons and RE axons in dCA1 blocked formation of fear extinction memory in our experiments. Interestingly, we observed that following transient chemogenetic inhibition of RE→dCA1 during the first fear extinction session, the impairment in extinction is evident not only during the subsequent extinction memory test but it also persists throughout the entire second extinction session. This persistent impairment of contextual fear extinction alludes to long-term extinction impairment induced by PSD-95 mutation in dCA1 observed in our former study. We found that contextual fear memory cannot be updated by the animals with dCA1 phosphorylation-deficient PSD-95(S73A) mutation even if they undergo six 30-minute contextual fear extinction sessions [36]. Hence, our data support the framework in which contextual fear extinction-induced and PSD-95-dependent synaptic plasticity in dCA1 is necessary to link the memories of contextual fear and contextual fear extinction, in order to persistently suppress contextual fear. The need for interaction between these two memory traces for fear extinction to occur, and the contribution of RE in this process, was also suggested by Totty and collaborators [20]. The authors observed the impairment of fear extinction memory *recall* upon optogenetic inhibition or electric stimulation of RE.

Previous work has found that RE is necessary for proper discrimination of contexts [26], and reductions in context discrimination might result in a relapse of fear [51]. However, more recent studies showed that the activity of RE axons in CA1 is not contextually modulated [24] and that 8-Hz stimulation of RE does not impair context recognition, although it affects recall of contextual fear extinction [20]. We also did not see impairments of context recognition after chemogenetic inhibition of RE→CA1. Hence, our work supports the notion that impaired fear extinction upon RE inactivation is a result of deficits in memory integration, rather than impaired recognition of the extinction context.

Recent studies showed that inhibiting the RE→CA1 pathway following CFC lengthens the duration of fearful freezing epochs [24]. In opposition to this finding, we observed no effect of RE→dCA1 manipulation on freezing frequency during fear memory recall. One of the reasons why we do not see the effect of chemogenetic inhibition of RE→CA1 on frequency of freezing upon fear memory recall could be the fact that our intensive CFC protocol with 5US resulted in very high freezing levels (approx. 85-90% of time), so it could not be further increased upon RE→CA1 inhibition. This hypothesis is supported by the experiment when animals had cannula implanted in the hippocampus and CFC resulted in freezing levels around 60%. In these groups, chemogenetic inhibition of RE axons in CA1 indeed increased freezing during contextual fear memory recall.

Beyond fear extinction, a separate line of research indicates the role of RE in spatial working memory that is used to guide future decisions [19,52–54]. For example, optogenetic inhibition of RE impairs accuracy of spatial choices in a delayed-non-match-to-position task in T-maze [55]. Here, in accordance with former studies, inhibition of the $RE^{\rightarrow CA1}$ neurons impaired accuracy of spatial choices during place avoidance as well as extinction of place preference and avoidance in close-to-ecological conditions of the IntelliCages. Interestingly, we did not see the effect of $RE^{\rightarrow CA1}$ inhibition on the accuracy of spatial choices during place

preference training. One of the reasons why place preference choices were not impaired in the animals with inhibited RE→dCA1 could be the fact that during this training mice stayed in a reward corner much longer, and visited the corner more often, as compared to all other tasks. Hence, since the intervals between the visits in the reward corner were shorter this task likely posed less demands on working memory.

Former studies linked the behavioral functions of RE with its impact on the coherence of theta oscillations between the hippocampus and prefrontal cortex [19,20,52]. Here we extend these findings demonstrating the impact of RE on training-induced molecular changes of the excitatory synapses in dCA1. Although synaptic plasticity in the hippocampus is broadly perceived as a key mechanism for memory formation, the alternative functions of this phenomenon have been also proposed. In particular, local genetic manipulations that impair synaptic function and plasticity in dCA1 affect spatial choice and incorporation of salience information into cognitive representations, rather than formation of cognitive maps and memory engrams [56–60]. In agreement with these assumptions, our study showed that RE input to dCA1 regulates extinction of context fear, aversion and preference, the processes that involve updating the context value. Since memories may be repeatedly reorganized upon recall [61,62], the molecular and cellular mechanisms involved in extinction of the existing fearful, aversive or appetitive memories provide excellent targets for memory impairment therapies. In particular, understanding the mechanisms that underlie contextual fear extinction may be relevant for post-traumatic stress disorder treatment, while place preference for drug use disorders.

Materials and Methods

Animals. C57BL/6J male mice, 7-9 weeks-old, were purchased from Białystok University, Poland. The Thy1GFP(M) (The Jackson Laboratory, JAX:007788, RRID:IMSR_JAX:007788) mutant mice were bred as heterozygotes at Nencki Institute and PCR genotyped (The Jackson Laboratory protocol). All of the mice for the behavioral studies were 4–7 months old at the time of training. The mice were housed alone and maintained on a 12 h light/dark cycle with food and water *ad libitum*. All experiments were undertaken in accordance with the Poland Animals (Scientific Procedures) Act and approved by the Local Ethics Committee in Warsaw, Poland (no. 529/2018).

Stereotactic surgery. Mice were anesthetized with isoflurane (5% for induction, 1.5-2.0% after) and fixed in the stereotactic frame (51503, Stoelting, Wood Dale, IL, USA). $AAV_{2.1}$ viruses [camk2a_mCherry (titer $7.5*10^8$/µl, from Karl Deisseroth's Lab); hSyn_hM4D(Gi)_mCherry ($4,59*10^9$/ul; Addgene plasmid #50475); hSyn_DiO_hM4Di-mCherry ($4.2*10^{10}$/ul; Addgene plasmid #44362)] were injected into RE (150 nl, coordinates from the Bregma: AP, -0.58 mm; ML, 0 mm; DV, 4.3 mm) and CAV2 virus [CAV2:Cre_GFP ($13.1*10^9$/ul, PVM Montpellier)] was injected into the dCA1 region of the hippocampus (500 nl per site, coordinates from the Bregma: AP, -2.1 mm; ML, ±1.1 mm; DV, -1.3 mm) [33]. We used beveled 26 gauge metal needle and 10 µl microsyringe (SGE010RNS, WPI, USA) connected to a microsyringe pump (UMP3, WPI, Sarasota, USA), and its controller (Micro4, WPI, Sarasota, USA) with an injection rate 0.1 µl/min. After injection, the needle was left in place for an additional 10 min to prevent unwanted spread of the vector. The AAV viruses were prepared by the Laboratory of Animal Models at Nencki Institute of Experimental Biology, Polish Academy of Sciences.

Cannula placement. After viral injection cannula was implanted. Bilateral cannulas (26GA, Plastics One) (coordinates from the Bregma: AP, -2.1 mm; ML, ± 1.1 mm; DV, -1.3 mm) [33]. Cement (Duracryl Plus,

SpofaDental) was used to anchor the guide cannula to the skull. Dummy cannulae (Plastics One) were inserted to keep the fiber guide from getting clogged. After the surgery, animals were allowed to recover for 21 days.

Contextual fear conditioning (CFC). Mice were trained in a conditioning chamber in a soundproof box (Med Associates Inc, St Albans, VT, USA). The chamber floor had a stainless steel grid for shock delivery. Before training, chambers were cleaned with 70% ethanol and paper towels were soaked in ethanol and placed under the grid floor.

On the day of contextual fear conditioning mice were brought to the room with a conditioning chamber 30 minutes before the training to acclimatize. Animals were placed in the chamber, and after a 148-second introductory period, a foot shock (2 seconds, 0.70 mA) (US) was presented. The shock was repeated five times, with intertrial interval of 90 seconds. Thirty seconds after the last shock, mice were returned to the home cage. Mice of the 5US group were sacrificed 24 hours after the initial training. The next day contextual fear was extinguished by re-exposing the animals to the conditioning chamber for 30 minutes without US presentation. Mice of the Extinction group were sacrificed right after the extinction session. To test the efficiency of extinction, mice were re-exposed to the training context 24 hours after the extinction session for an additional 30 minutes.

A video camera was fixed inside the door of the sound attenuating box, for the behavior to be recorded and scored. Freezing behavior (defined as complete lack of movement, except respiration) and locomotor activity of mice were automatically scored. The experimenters were blind to the experimental groups.

CNO administration. For intraperitoneal (i.p.) injections, Clozapine N-Oxide (CNO) was dissolved in 0.9% saline. 3 mg/kg CNO was injected 30 minutes prior to the contextual fear memory extinction training and spatial training in the IntelliCages. To avoid multiple i.p. injections during the preference and avoidance extinction tests in the IntelliCages, CNO was dissolved in drinking water available in both cage corners (0.012 mg/ml) resulting in daily CNO consumption of approximately 3 mg/kg [34] .

Place preference and avoidance in the IntelliCages. Three weeks after stereotactic surgery (CA1:CAV2-Cre-GFP and RE:hSyn-Dio-hM4Di-mCherry), mice were divided in two experimental groups - saline (n = 12) and CNO (n = 12), and transferred in two IntelliCages (NewBehavior, https://www.tse-systems.com/; 20.5 cm tall, 40 × 58 cm at the top, and 55 × 37.5 cm at the base). The cages were equipped with two conditioning chambers (active corners). Mice entered the corners by passing through a plastic ring (outer ring, 50 mm diameter; inner ring, 30 mm diameter; 20 mm depth into the outer ring) and they could access the bottles with reward if they performed nosepokes to doors covering the access to the bottles. The system recorded the number and duration of visits, nosepokes and licks in active corners.

In the IntelliCages, mice underwent seven days of adaptation, place preference training (1 day), preference extinction (4 days), place avoidance (1 day) and avoidance extinction (3 days). During habituation mice had access only to water in both cage corners. During place preference training water in one corner (less visited corner during adaptation phase) was replaced with sucrose solution (5%, Sigma-Aldrich). During preference extinction, sucrose solution was replaced with water. During place avoidance, quinine solution (3 g/l, Sigma-Aldrich) was put in one corner (the most prefered corner during the last day before avoidance training) for 24 hours. Finally, during the extinction of place avoidance, quinine was replaced by water. Frequency of visits in the training corner was used as a measure of place preference and avoidance.

Immunostaining. Mice were anesthetized and perfused with 4% PFA (Sigma Aldrich) in PBS buffer, pH 7.5 (Medicago). Coronal brain sections (40 µm) were prepared (Cryostats Leica CM1950) and stored at -20°C in PBSAF [PBS, 15% sucrose (POCH), 30% ethylene glycol (Sigma-Aldrich), and 0.05% NaN3 (SigmaAldrich)].

The sections were washed three times in a PBS buffer and incubated in blocking solution [5% NDS (Jackson ImmunoREsearch)/0.3% Triton X-100 (Sigma Aldrich) in PBS] for 1h at room temperature. Next, sections were incubated in 4°C overnight with primary antibodies directed against PSD-95 (Millipore, MAB 1598). Next, the slices were washed in 0.3% Triton X-100 in PBS and incubated with a secondary antibody bound with Alexa Fluor 647 (Invitrogen, A31571). The sections were washed 3 times in PBS, mounted on glass microscope slides (Thermo Fisher Scientific) and coverslipped with Fluoromount-G medium with DAPI for fluorescence (Invitrogen, 00-4959-52).

Confocal microscopy and image quantification. The microphotographs of fluorescent immunostaining, axon terminals and dendritic spines in Thy1-GFP mice were taken on Zeiss Spinning Disc confocal microscope (63X oil objective and 1.0 optovar) (Zeiss, Göttingen, Germany). Images (z-stack; 260 nm distance) were taken of 6 hippocampi of each animal in dCA1 stratum oriens (SO), medial part of radiatum (SR) and lacunosum-moleculare (SLM) (AP, Bregma from -1.7 to 2.06). We took microphotographs of secondary dendrites, 5-6 dendrites per mouse.

All image Z-series were first processed with Huygens Professional deconvolution software to reduce background and to extract in a statistically reliable way all relevant information from this image series. We analyzed these images with Fiji and Python software using custom-written scripts to mark and count dendritic spines with co-localization with PSD-95-positive puncta and dendritic contact with axon terminals from *nucleus reuniens* (RE). A contact is the physical apposition of processes of two different neurons. We searched for buttons of the mCherry labeled axons/fibers in contact with GFP labeled dendrites. Buttons were defined as any swelling of an en passant fiber with diameter at least three times bigger than axon. A contact required observation of a button on mCherry labeled axon in immediate apposition (in one microphotography) to GFP labeled dendritic protrusions. The density and mean gray value of PSD-95-positive puncta and their co-localization were analyzed using Fiji software.

Serial Block-FaceScanning Electron Microscopy (SBFSEM). Mice were transcardially perfused with cold phosphate buffer pH 7.4, followed by 0.5% EM-grade glutaraldehyde (G5882 Sigma-Aldrich) with 2% PFA in phosphate buffer pH 7.4 and postfixed overnight in the same solution. Brains were then taken out of the fixative and cut on a vibratome (Leica VT 1200) into 100 µm slices. Slices were kept in phosphate buffer pH 7.4, with 0.1% sodium azide in 4°C. Then, slices were washed 3 times in cold phosphate buffer and postfixed with a solution of 2% osmium tetroxide (#75632 Sigma-Aldrich) and 1.5% potassium ferrocyanide (P3289 Sigma-Aldrich) in 0.1 M phosphate buffer pH 7.4 for 60 min on ice. Next, samples were rinsed 5 × 3 min with double distilled water (ddH2O) and subsequently exposed to 1% aqueous thiocarbohydrazide (TCH) (#88535 Sigma) solution for 20 min. Samples were then washed 5 × 3 min with ddH2O and stained with osmium tetroxide (1% osmium tetroxide in ddH_2O) for 30 min in RT. Afterward, slices were rinsed 5 × 3 min with ddH2O and incubated in 1% aqueous solution of uranyl acetate overnight in 4°C. The next day, slices were rinsed 5 × 3 min with ddH2O, incubated with lead aspartate solution for 30 min in 60°C and then washed 5 × 3 min with ddH2O and dehydration was performed using graded dilutions of ice-cold ethanol (30%, 50%, 70%, 80%, 90%, and 2 × 100% ethanol, 5 min each). Then slices were infiltrated with Durcupan resin and flat embedded between Aclar

sheets (Ted Pella #10501-10). Next Aclar layers were separated from the resin embedded samples, and the dCA1 region was cut out with a razorblade. Squares of approximately 1 × 1 × 1 mm were attached to aluminium pins (Gatan metal rivets, Oxford instruments) with very little amount of cyanacrylate glue. Next, samples were mounted to the ultramicrotome to cut 1 µm thick slices. Slices were transferred on a microscope slide, briefly stained with 1% toluidine blue in 5% borate and observed under a light microscope to confirm the region of interest (ROI). Next, samples were grounded with silver paint (Ted Pella, 16062-15) and left for drying for 4 – 12 hours, before the specimens were mounted into the 3View2 chamber.

SBEM imaging and 3D reconstructions. Samples were imaged with Zeiss SigmaVP (Zeiss, Oberkochen, Germany) scanning electron microscope equipped with 3View2 GATAN chamber using a backscatter electron detector. Scans were taken in the middle portion of dCA1 SO. From each sample, 200 sections were collected (thickness 60 nm). Imaging settings: high vacuum with EHT 2.8 kV, aperture: 20 µm, pixel dwell time: 3 µs, pixel size: 5 – 6.2 nm. Scans were aligned using the ImageJ software (ImageJ → Plugins → Registration → StackReg) and saved as .tiff image sequence. Next, aligned scans were imported to Reconstruct software, available at http://synapses.clm.utexas.edu/tools/reconstruct/reconstruct.stm (Synapse Web REconstruct, RRID:SCR_002716). Dendritic spine density was analyzed from 3 bricks per animal with the unbiased brick method [35] per tissue volume. Brick dimensions 3 × 3 × 3 µm were chosen to exceed the length of the largest profiles in the data sets at least twice. To calculate the density of dendritic spines, the total volume of large tissue discontinuities was subtracted from the volume of the brick.

A structure was considered to be a dendritic spine when it was a definite protrusion from the dendrite, with electron-dense material (representing postsynaptic part of the synapse, PSD) on the part of the membrane that opposed an axonal button with at least 3 vesicles within a 50-nm distance from the cellular membrane facing the spine. For 3D reconstructions, PSDs and dendritic spines in one brick were reconstructed for each sample. PSDs were first reconstructed and second, their dendritic spines were outlined. To separate dendritic spine necks from the dendrites, a cut-off plane was used approximating where the dendritic surface would be without the dendritic spine. PSD volume was measured by outlining dark, electron-dense areas on each PSD-containing section (45). The PSD area was measured manually according to the Reconstruct manual. All non-synaptic protrusions were omitted in this analysis. For multi-synaptic spines, the PSD areas and volumes were summed.

Electrophysiology. Mice were deeply anesthetized with isoflurane, decapitated and the brains were rapidly dissected and transferred into ice-cold cutting artificial cerebrospinal fluid (ACSF) consisting of (in mM): 87 NaCl, 2.5 KCl, 1.25 NaH_2PO_4, 25 $NaHCO_3$, 0.5 $CaCl_2$, 7 $MgSO_4$, 20 D-glucose, 75 saccharose equilibrated with carbogen (5% CO_2/95% O_2). The brain was cut to two hemispheres and 350 µm thick coronal brain slices were cut in ice-cold cutting ACSF with Leica VT100S vibratome. Slices were then incubated for 15 min in cutting ACSF at 32°C. Next the slices were transferred to recording ACSF containing (in mM): 125 NaCl, 2.5 KCl, 1.25 NaH_2PO_4, 25 $NaHCO_3$, 2.5 $CaCl_2$, 1.5 $MgSO_4$, 20 D-glucose equilibrated with carbogen and incubated for minimum 1 hour at RT.

Extracellular field potential recordings were recorded in a submerged chamber perfused with recording ACSF in RT. The potentials were evoked with a Stimulus Isolator (A.M.P.I Isoflex) with a concentric bipolar electrode (FHC, CBARC75) placed in the SO, SR, or SLM of CA3 depending on the experiment. The stimulating pulses were delivered at 0.1 Hz and the pulse duration was 0.3 ms. REcording electrodes

(resistance 1-4 MΩ) were pulled from borosilicate glass (WPI, 1B120F-4) with a micropipette puller (Sutter Instruments, P-1000) and filled with recording ACSF. The recording electrodes were placed in the SO, SR, or SLM of the dorsal CA1 area depending on the measurement. Simultaneously, a second recording electrode was placed in the stratum pyramidale to measure population spikes. For each slice the recordings were done in both SO, and SR. Field excitatory synaptic potentials (fEPSPs) were always recorded first in SR and then the stimulating and recording electrodes were moved to SO and SLM. Recordings were acquired with MultiClamp 700B (Molecular Devices, California, USA), Digidata 1550B (Molecular Devices, California, USA) and Clampex 10.0 software (Molecular Devices, California, USA). Input/output curves were obtained by increasing stimulation intensity by 25 μA in the range of 0-300 μA. Input/Output curves were analyzed with AxoGraph 1.7.4 software (Axon Instruments, U.S.A). The slope of fEPSP, relative amplitude of population spikes and fiber volley were measured.

Statistics. Analysis was performed using Graphpad Prism 8. All the statistical details of experiments can be found in the legends of the figures. Data with normal distribution are presented as mean ± standard error of the mean (SEM) or as median ± interquartile range (IQR) for the population with non-normal distribution. When the data met the assumptions of parametric statistical tests, results were analyzed by one- or repeated measures two-way ANOVA, followed by Tukey's or Fisher's *post hoc* tests, where applicable. Areas of axonal button, dendritic spines and PSD-95 puncta did not follow normal distributions and were analyzed with the Kruskal-Wallis test. Differences in means were considered statistically significant at $p < 0.05$.

Acknowledgments, Funding and Disclosure

This work was supported by a National Science Center (Poland) [PRELUDIUM Grant No. 2016/23/N/NZ4/03304 to MZ; and MAESTRO grant No. 2020/38/A/NZ4/00483 to KR]. The project was carried out with the use of CePT infrastructure financed by the European Union - The European Regional Development Fund within the Operational Program "Innovative economy" for 2007-2013.

The funders had no role in study design, data collection and analysis, decision to publish, or preparation of the manuscript.

DECLARATION OF INTEREST

Authors report no financial interests or conflicts of interest.

INCLUSION AND DIVERSITY

While citing references scientifically relevant for this work, we also actively worked to promote gender balance in our reference list. We support inclusive, diverse, and equitable conduct of research.

LITERATURE

1. Lissek S, Kaczkurkin AN, Rabin S, Geraci M, Pine DS, Grillon C. Generalized anxiety disorder is associated with overgeneralization of classically conditioned fear. Biol Psychiatry. 2014;75: 909–915.

doi:10.1016/j.biopsych.2013.07.025

2. Garfinkel SN, Abelson JL, King AP, Sripada RK, Wang X, Gaines LM, et al. Impaired contextual modulation of memories in PTSD: an fMRI and psychophysiological study of extinction retention and fear renewal. J Neurosci. 2014;34: 13435–13443. doi:10.1523/JNEUROSCI.4287-13.2014

3. Grodin EN, Sussman L, Sundby K, Brennan GM, Diazgranados N, Heilig M, et al. Neural Correlates of Compulsive Alcohol Seeking in Heavy Drinkers. Biol Psychiatry Cogn Neurosci Neuroimaging. 2018;3: 1022–1031. doi:10.1016/j.bpsc.2018.06.009

4. Maren S, Phan KL, Liberzon I. The contextual brain: implications for fear conditioning, extinction and psychopathology. Nat Rev Neurosci. 2013;14: 417–428. doi:10.1038/nrn3492

5. Ji J, Maren S. Hippocampal involvement in contextual modulation of fear extinction. Hippocampus. 2007;17: 749–758. doi:https://doi.org/10.1002/hipo.20331

6. Maren S, Quirk GJ. Neuronal signalling of fear memory. Nat Rev Neurosci. 2004;5: 844–852. doi:10.1038/nrn1535

7. Myers KM, Davis M. Behavioral and Neural Analysis of Extinction. Neuron. 2002;36: 567–584. doi:10.1016/S0896-6273(02)01064-4

8. Orsini CA, Maren S. Neural and cellular mechanisms of fear and extinction memory formation. Neurosci Biobehav Rev. 2012;36: 1773–1802. doi:10.1016/j.neubiorev.2011.12.014

9. Venkataraman A, Dias BG. Expanding the canon: An inclusive neurobiology of thalamic and subthalamic fear circuits. Neuropharmacology. 2023;226: 109380. doi:10.1016/j.neuropharm.2022.109380

10. Cassel J-C, Pereira de Vasconcelos A, Loureiro M, Cholvin T, Dalrymple-Alford JC, Vertes RP. The reuniens and rhomboid nuclei: Neuroanatomy, electrophysiological characteristics and behavioral implications. Progress in Neurobiology. 2013;111: 34–52. doi:10.1016/j.pneurobio.2013.08.006

11. Hoover WB, Vertes RP. Collateral projections from nucleus reuniens of thalamus to hippocampus and medial prefrontal cortex in the rat: a single and double retrograde fluorescent labeling study. Brain Struct Funct. 2012;217: 191–209. doi:10.1007/s00429-011-0345-6

12. Varela C, Kumar S, Yang JY, Wilson MA. Anatomical substrates for direct interactions between hippocampus, medial prefrontal cortex, and the thalamic nucleus reuniens. Brain Struct Funct. 2014;219: 911–929. doi:10.1007/s00429-013-0543-5

13. Vertes RP, Hoover WB, Szigeti-Buck K, Leranth C. Nucleus reuniens of the midline thalamus: Link between the medial prefrontal cortex and the hippocampus. Brain Research Bulletin. 2007;71: 601–609. doi:10.1016/j.brainresbull.2006.12.002

14. Goswamee P, Leggett E, McQuiston AR. Nucleus Reuniens Afferents in Hippocampus Modulate CA1 Network Function via Monosynaptic Excitation and Polysynaptic Inhibition. Frontiers in Cellular Neuroscience. 2021;15. Available: https://www.frontiersin.org/articles/10.3389/fncel.2021.660897

15. Dolleman-Van der Weel MJ, Lopes da Silva FH, Witter MP. Nucleus Reuniens Thalami Modulates Activity in Hippocampal Field CA1 through Excitatory and Inhibitory Mechanisms. J Neurosci. 1997;17: 5640–5650. doi:10.1523/JNEUROSCI.17-14-05640.1997

16. Wouterlood FG, Saldana E, Witter MP. Projection from the nucleus reuniens thalami to the hippocampal region: Light and electron microscopic tracing study in the rat with the anterograde tracerPhaseolus vulgaris-leucoagglutinin. J Comp Neurol. 1990;296: 179–203. doi:10.1002/cne.902960202

17. Jayachandran M, Viena TD, Garcia A, Veliz AV, Leyva S, Roldan V, et al. Nucleus reuniens transiently synchronizes memory networks at beta frequencies. Nat Commun. 2023;14: 4326. doi:10.1038/s41467-023-40044-z
18. Dolleman-van der Weel MJ, Griffin AL, Ito HT, Shapiro ML, Witter MP, Vertes RP, et al. The nucleus reuniens of the thalamus sits at the nexus of a hippocampus and medial prefrontal cortex circuit enabling memory and behavior. Learn Mem. 2019;26: 191–205. doi:10.1101/lm.048389.118
19. Griffin AL. The nucleus reuniens orchestrates prefrontal-hippocampal synchrony during spatial working memory. Neurosci Biobehav Rev. 2021;128: 415–420. doi:10.1016/j.neubiorev.2021.05.033
20. Totty MS, Tuna T, Ramanathan KR, Jin J, Peters SE, Maren S. Thalamic nucleus reuniens coordinates prefrontal-hippocampal synchrony to suppress extinguished fear. Nat Commun. 2023;14: 6565. doi:10.1038/s41467-023-42315-1
21. Ramanathan KR, Jin J, Giustino TF, Payne MR, Maren S. Prefrontal projections to the thalamic nucleus reuniens mediate fear extinction. Nat Commun. 2018;9: 4527. doi:10.1038/s41467-018-06970-z
22. Silva BA, Burns AM, Gräff J. A cFos activation map of remote fear memory attenuation. Psychopharmacology. 2019;236: 369–381. doi:10.1007/s00213-018-5000-y
23. Silva BA, Astori S, Burns AM, Heiser H, van den Heuvel L, Santoni G, et al. A thalamo-amygdalar circuit underlying the extinction of remote fear memories. Nat Neurosci. 2021;24: 964–974. doi:10.1038/s41593-021-00856-y
24. Ratigan HC, Krishnan S, Smith S, Sheffield MEJ. A thalamic-hippocampal CA1 signal for contextual fear memory suppression, extinction, and discrimination. Nat Commun. 2023;14: 6758. doi:10.1038/s41467-023-42429-6
25. Troyner F, Bicca MA, Bertoglio LJ. Nucleus reuniens of the thalamus controls fear memory intensity, specificity and long-term maintenance during consolidation. Hippocampus. 2018;28: 602–616. doi:10.1002/hipo.22964
26. Xu W, Sudhof TC. A Neural Circuit for Memory Specificity and Generalization. Science. 2013;339: 1290–1295. doi:10.1126/science.1229534
27. Rozeske RR, Valerio S, Chaudun F, Herry C. Prefrontal neuronal circuits of contextual fear conditioning. Genes, Brain and Behavior. 2015;14: 22–36. doi:10.1111/gbb.12181
28. Zelikowsky M, Hersman S, Chawla MK, Barnes CA, Fanselow MS. Neuronal Ensembles in Amygdala, Hippocampus, and Prefrontal Cortex Track Differential Components of Contextual Fear. Journal of Neuroscience. 2014;34: 8462–8466. doi:10.1523/JNEUROSCI.3624-13.2014
29. Armbruster BN, Li X, Pausch MH, Herlitze S, Roth BL. Evolving the lock to fit the key to create a family of G protein-coupled receptors potently activated by an inert ligand. Proc Natl Acad Sci U S A. 2007;104: 5163–5168. doi:10.1073/pnas.0700293104
30. Feng G, Mellor RH, Bernstein M, Keller-Peck C, Nguyen QT, Wallace M, et al. Imaging Neuronal Subsets in Transgenic Mice Expressing Multiple Spectral Variants of GFP. Neuron. 2000;28: 41–51. doi:10.1016/S0896-6273(00)00084-2
31. Denk W, Horstmann H. Serial Block-Face Scanning Electron Microscopy to Reconstruct Three-Dimensional Tissue Nanostructure. PLoS Biol. 2004;2. doi:10.1371/journal.pbio.0020329
32. Śliwińska MA, Cały A, Szymański J, Radwańska K. Serial Block-Face Scanning Electron Microscopy (SBEM) for the Study of Dendritic Spines. J Vis Exp. 2021. doi:10.3791/62712

33. Paxinos and Franklin's the Mouse Brain in Stereotaxic Coordinates, Compact - 5th Edition. [cited 3 Jul 2021]. Available: https://www.elsevier.com/books/paxinos-and-franklins-the-mouse-brain-in-stereotaxic-coordinates-compact/franklin/978-0-12-816159-3
34. Zhan J, Komal R, Keenan WT, Hattar S, Fernandez DC. Non-invasive Strategies for Chronic Manipulation of DREADD-controlled Neuronal Activity. J Vis Exp. 2019; 10.3791/59439. doi:10.3791/59439
35. Fiala JC, Harris KM. Extending unbiased stereology of brain ultrastructure to three-dimensional volumes. J Am Med Inform Assoc. 2001;8: 1–16. doi:10.1136/jamia.2001.0080001
36. Ziółkowska M, Borczyk M, Cały A, Tomaszewski KF, Nowacka A, Nalberczak-Skóra M, et al. Phosphorylation of PSD-95 at serine 73 in dCA1 is required for extinction of contextual fear. PLoS Biol. 2023;21: e3002106. doi:10.1371/journal.pbio.3002106
37. Herkenham M. The connections of the nucleus reuniens thalami: evidence for a direct thalamo-hippocampal pathway in the rat. J Comp Neurol. 1978;177: 589–610. doi:10.1002/cne.901770405
38. Kajiwara R, Wouterlood FG, Sah A, Boekel AJ, Baks-te Bulte LTG, Witter MP. Convergence of entorhinal and CA3 inputs onto pyramidal neurons and interneurons in hippocampal area CA1—An anatomical study in the rat. Hippocampus. 2008;18: 266–280. doi:10.1002/hipo.20385
39. Vertes RP, Hoover WB, Do Valle AC, Sherman A, Rodriguez JJ. Efferent projections of reuniens and rhomboid nuclei of the thalamus in the rat. J Comp Neurol. 2006;499: 768–796. doi:10.1002/cne.21135
40. Abraham WC, Jones OD, Glanzman DL. Is plasticity of synapses the mechanism of long-term memory storage? npj Sci Learn. 2019;4: 9. doi:10.1038/s41539-019-0048-y
41. Bliss TVP, Collingridge GL. A synaptic model of memory: long-term potentiation in the hippocampus. Nature. 1993;361: 31–39. doi:10.1038/361031a0
42. Morris RGM, Moser EI, Riedel G, Martin SJ, Sandin J, Day M, et al. Elements of a neurobiological theory of the hippocampus: the role of activity-dependent synaptic plasticity in memory. Bliss TVP, Collingridge GL, Morris RGM, editors. Phil Trans R Soc Lond B. 2003;358: 773–786. doi:10.1098/rstb.2002.1264
43. Radwanska K, Medvedev NI, Pereira GS, Engmann O, Thiede N, Moraes MFD, et al. Mechanism for long-term memory formation when synaptic strengthening is impaired. Proc Natl Acad Sci U S A. 2011;108: 18471–18475. doi:10.1073/pnas.1109680108
44. Schuette PJ, Reis FMCV, Maesta-Pereira S, Chakerian M, Torossian A, Blair GJ, et al. Long-Term Characterization of Hippocampal Remapping during Contextual Fear Acquisition and Extinction. J Neurosci. 2020;40: 8329–8342. doi:10.1523/JNEUROSCI.1022-20.2020
45. Stansley BJ, Fisher NM, Gogliotti RG, Lindsley CW, Conn PJ, Niswender CM. Contextual Fear Extinction Induces Hippocampal Metaplasticity Mediated by Metabotropic Glutamate Receptor 5. Cerebral Cortex. 2018;28: 4291–4304. doi:10.1093/cercor/bhx282
46. Garín-Aguilar ME, Díaz-Cintra S, Quirarte GL, Aguilar-Vázquez A, Medina AC, Prado-Alcalá RA. Extinction procedure induces pruning of dendritic spines in CA1 hippocampal field depending on strength of training in rats. Front Behav Neurosci. 2012;6. doi:10.3389/fnbeh.2012.00012
47. Troyner F, Bertoglio LJ. Nucleus reuniens of the thalamus controls fear memory reconsolidation. Neurobiology of Learning and Memory. 2021;177: 107343. doi:10.1016/j.nlm.2020.107343
48. Ramanathan KR, Maren S. Nucleus reuniens mediates the extinction of contextual fear conditioning. Behav Brain Res. 2019;374: 112114. doi:10.1016/j.bbr.2019.112114

49. Vasudevan K, Ramanathan KR, Vierkant V, Maren S. Nucleus reuniens inactivation does not impair consolidation or reconsolidation of fear extinction. Learn Mem. 2022;29: 216–222. doi:10.1101/lm.053611.122
50. Vetere G, Kenney JW, Tran LM, Xia F, Steadman PE, Parkinson J, et al. Chemogenetic Interrogation of a Brain-wide Fear Memory Network in Mice. Neuron. 2017;94: 363-374.e4. doi:10.1016/j.neuron.2017.03.037
51. Bouton ME, Bolles RC. Contextual control of the extinction of conditioned fear. Learning and Motivation. 1979;10: 445–466. doi:10.1016/0023-9690(79)90057-2
52. Ito HT, Zhang S-J, Witter MP, Moser EI, Moser M-B. A prefrontal–thalamo–hippocampal circuit for goal-directed spatial navigation. Nature. 2015;522: 50–55. doi:10.1038/nature14396
53. Stout JJ, Hallock HL, George AE, Adiraju SS, Griffin AL. The ventral midline thalamus coordinates prefrontal–hippocampal neural synchrony during vicarious trial and error. Sci Rep. 2022;12: 10940. doi:10.1038/s41598-022-14707-8
54. Mei H, Logothetis NK, Eschenko O. The activity of thalamic nucleus reuniens is critical for memory retrieval, but not essential for the early phase of “off-line” consolidation. Learn Mem. 2018;25: 129–137. doi:10.1101/lm.047134.117
55. Maisson DJ-N, Gemzik ZM, Griffin AL. Optogenetic suppression of the nucleus reuniens selectively impairs encoding during spatial working memory. Neurobiology of Learning and Memory. 2018;155: 78–85. doi:10.1016/j.nlm.2018.06.010
56. Bannerman DM, Bus T, Taylor A, Sanderson DJ, Schwarz I, Jensen V, et al. Dissecting spatial knowledge from spatial choice by hippocampal NMDA receptor deletion. Nat Neurosci. 2012;15: 1153–1159. doi:10.1038/nn.3166
57. Bannerman DM, Sprengel R, Sanderson DJ, McHugh SB, Rawlins JNP, Monyer H, et al. Hippocampal synaptic plasticity, spatial memory and anxiety. Nature Reviews Neuroscience. 2014;15: 181–192. doi:10.1038/nrn3677
58. Hirsch SJ, Regmi NL, Birnbaum SG, Greene RW. CA1-specific deletion of NMDA receptors induces abnormal renewal of a learned fear response. Hippocampus. 2015;25: 1374–1379. doi:10.1002/hipo.22457
59. Cały A, Śliwińska MA, Ziółkowska M, Łukasiewicz K, Pagano R, Dzik JM, et al. PSD-95 in CA1 area regulates spatial choice depending on age. J Neurosci. 2021 [cited 26 Jan 2021]. doi:10.1523/JNEUROSCI.1996-20.2020
60. Kaganovsky K, Plitt MH, Yang R, Sando R, Giocomo LM, Ding JB, et al. Dissociating encoding of memory and salience by manipulating long-term synaptic potentiation. bioRxiv; 2022. p. 2022.01.04.474865. doi:10.1101/2022.01.04.474865
61. Nader K, Schafe GE, Le Doux JE. Fear memories require protein synthesis in the amygdala for reconsolidation after retrieval. Nature. 2000;406: 722–726. doi:10.1038/35021052
62. Schafe GE, Nader K, Blair HT, LeDoux JE. Memory consolidation of Pavlovian fear conditioning: a cellular and molecular perspective. Trends in Neurosciences. 2001;24: 540–546. doi:10.1016/S0166-2236(00)01969-X

Supplementary Materials

Projections from thalamic nucleus reuniens to hippocampal CA1 area enable context value updating

Authors

Magdalena Ziółkowska, Narges Sotoudeh, Anna Cały, Monika Puchalska, Roberto Pagano[&], Małgorzata Alicja Śliwińska[#], Ahmad Salamian and Kasia Radwanska*****

Affiliation

Laboratory of Molecular Basis of Behavior, Nencki Institute of Experimental Biology of Polish Academy of Sciences, 3 Pasteur St., Warsaw 02-093, Poland.

[&] currently Laboratory of Molecular and Cellular Neurobiology, International Institute of Molecular and Cell Biology, Warsaw, Poland

[#] currently Electron Microscopy Platform & Bio Imaging Core at VIB-KU Leuven Center for Brain and Disease Research, and Department of Neurosciences at KU Leuven, Campus Gasthuisberg, building O&N5, Herestraat 49 box 602, 3000 Leuven, Belgium.

***Corresponding author:** Kasia Radwanska, Ph.D., Laboratory of Molecular Basis of Behavior, the Nencki Institute of Experimental Biology of Polish Academy of Sciences, 3 Pasteur St., Warsaw 02-093, Poland; e-mail: k.radwanska@nencki.edu.pl; tel: +48 501 736 942.

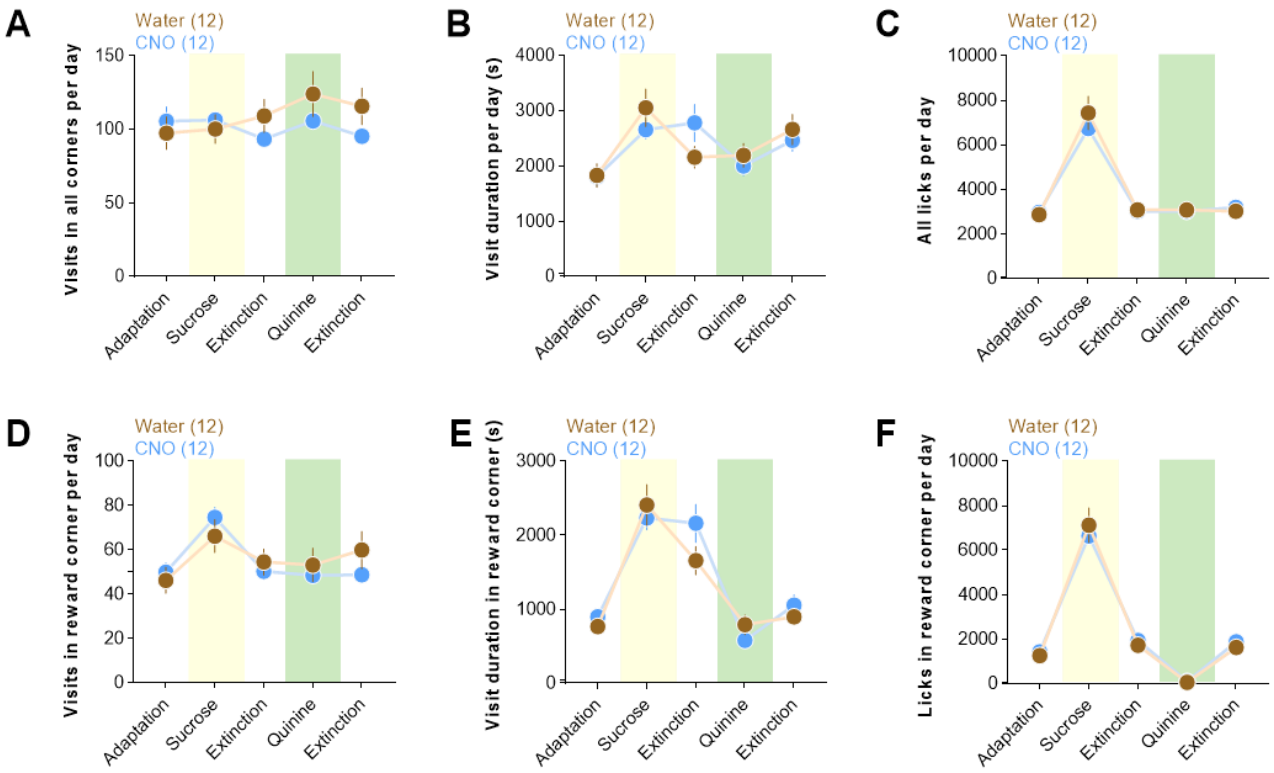

Supplementary Figure 1. Chemogenetic inhibition of the RE→dCA1 pathway does not affect general mice activity in the IntelliCages.

Mice had stereotactic injection of $AAV_{2.1}$:hSyn_DIO_hM4_mCherry in RE and CAV_2:camk2a_Cre_GFP in dCA1. Three weeks after the surgery and virus expression, they were trained in IntelliCages - place preference training (Sucrose) was followed by preference extinction, place avoidance (Quinine) and avoidance extinction. During training and extinction sessions CNO mice had CNO dissolved in drinking water.

(A-C) Summary of data showing total number of visits (RM two-way ANOVA, effect of CNO: $F(1, 22) = 0.468$, $p = 0.501$; effect of time: $F(3,29, 72,4) = 2.10$, $p = 0.101$), visit duration (RM two-way ANOVA, effect of CNO: $F(1, 22) = 0.020$, $p = 0.889$; effect of time: $F(3,36, 73,9) = 12.9$, $p < 0.001$) and licks in active cage corners (RM two-way ANOVA, effect of CNO: $F(1, 22) = 0.124$, $p = 0.728$; effect of time: $F(1,16, 25,5) = 118$, $p < 0.001$).

(D-F) Summary of data showing mice activity in reward corner: number of visits (RM two-way ANOVA, effect of CNO: $F(1, 22) = 0.064$, $p = 0.801$; effect of time: $F(2,99, 65,8) = 9.59$, $p < 0.001$), visit duration (RM two-way ANOVA, effect of CNO: $F(1, 22) = 0.204$, $p = 0.656$; effect of time: $F(2,79, 61,4) = 75.9$, $p <0.001$) and licks in “reward” corner (RM two-way ANOVA, effect of CNO: $F(1, 22) = 0.029$, $p = 0.866$; effect of time: $F(1,41, 31,0) = 177$, $p < 0.001$).